Journal of proteome research

Open Access

pubs.acs.org/jpr

Article

Proteomics and Metabolomics Analyses Reveal a Dynamic Landscape of Coal Workers' Pneumoconiosis: An Insight into Disease Progression

Yangyang Wei, Zhenzhen Jia, Jing Ma, Wei Zhang, Hui Li, Juan Wu, Xiaojing Wang, Xiao Yu, Yiwei Shi,* Xiaomei Kong,* and Min Pang*

Cite This: *J. Proteome Res.* 2025, 24, 1715−1731

Read Online

ACCESS | Metrics & More | Article Recommendations | Supporting Information

ABSTRACT: Coal worker's pneumoconiosis (CWP) is characterized by chronic inflammation and pulmonary fibrosis. The key factor contributing to the incurability of CWP is the unclear pathogenesis. This study explored the characteristic changes in proteomics and metabolomics of early and advanced CWP patients through proteomics and metabolomics techniques. Proteomics identified proteins that change with the progression of CWP, with significant enrichment in the TGF-β signaling pathway and autoimmune disease pathways. Metabolomics revealed the metabolic characteristics of CWP at different stages. These metabolites mainly include changes in amino acid metabolism, unsaturated fatty acid synthesis, and related metabolites. Integrated analysis found that ABC transporters are a shared pathway among the three groups, and ABCD2 is involved in the ABC transporter pathway. In the subsequent independent sample verification analysis, consistent with proteomics experiments, compared to the CM group, FMOD expression level was upregulated in the NIC group. TFR expression level was consistently downregulated in both the IC and NIC groups. Additionally, ABCD2 increased in the IC group but decreased in the NIC group. In summary, this study revealed the metabolic characteristics of CWP at different stages. These findings may provide valuable insights for the early prediction, diagnosis, and treatment of CWP.

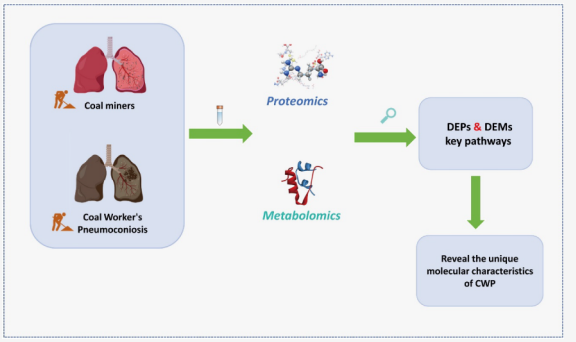

KEYWORDS: *coal worker's pneumoconiosis, broncho-alveolar lavage fluid, proteomics, metabolomics*

INTRODUCTION

Coal worker's pneumoconiosis (CWP), a prevalent occupational disease stemming from chronic inhalation of coal dust among miners,[1] leads to the accumulation of immune cells in lung regions proximal to bronchioles and alveoli, ultimately resulting in pulmonary fibrosis and immune dysfunction.[2,3] This condition poses a significant public health challenge globally, particularly in developing nations where coal serves as the primary energy source.[4] Although the setting of exposure limits and the improvement of mining environment have greatly reduced the incidence of CWP, recent research results show that the incidence of CWP is rebounding.[5] Meanwhile, multiple studies have pointed out that the existence of CWP can lead to a significant increase in patient mortality.[6,7] The increasing incidence of CWP and high risk have renewed the attention of researchers on the occupational health of coal miners.

The diagnosis of CWP relies on dust exposure history and imaging examination.[8] The occurrence of CWP requires long-term exposure to coal dust, and there is a lack of specific symptoms in the early stages of CWP.[9] The long time span of exposure history, combined with the concealment of early clinical symptoms, greatly reduces the early detection rate of CWP.[10,11] In terms of treatment, there is currently a lack of effective therapeutic measures for CWP patients. In the early stage of CWP, targeted supportive treatments such as bronchodilators and oxygen inhalation can be applied.[12] For patients in the end stage of CWP, lung transplantation is the only option.[13] Continuing to deeply explore the key mechanisms underlying the occurrence and development of CWP and searching for reliable biomarkers that can be used for early diagnosis of CWP are crucial for the current prevention and treatment of CWP.

Thanks to the rapid advancement of high-throughput technology in bioinformatics, researchers can now analyze various tissues, including tissue,[14] plasma, serum,[15] follicular fluid,[16] and bronchoalveolar lavage fluid,[17] to gain a more

Received: September 6, 2024
Revised: February 13, 2025
Accepted: February 14, 2025
Published: March 4, 2025

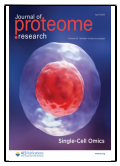

https://doi.org/10.1021/acs.jproteome.4c00715
J. Proteome Res. 2025, 24, 1715−1731

precise understanding of the normal physiological state of cells, intercellular material transfer, and corresponding changes caused by pathological conditions. Besides exploring basic mechanisms, multiomics technology is increasingly being applied in disease treatment and prognosis. In the realm of systems medicine, omics technologies enable comprehensive elucidation of molecular alterations, offering profound insights into disease pathogenesis and advancing precision medicine strategies for lung diseases.[18,19] Proteins serve as vehicles for gene function, while metabolites lie downstream of protein regulatory networks. The intricate interplay between genes, environment, and their interactions can be dissected through quantitative analysis of proteins and metabolites, yielding a treasure trove of "translatable" diagnostic and therapeutic targets. Currently, metabolomics and proteomics analyses have been widely used in the study of complex systems.[20,21] However, most studies tend to focus on the analysis of a single omics, limiting our comprehensive understanding of complex biological processes. The integration of multiple omics reveals molecular changes more comprehensively, helping us to deeply understand the pathogenesis during disease progression and providing new insights for early diagnosis and intervention strategies of diseases.[22]

Over the past decade, omics studies pertaining to lung diseases have garnered widespread attention, encompassing an expanding array of tissue samples. Bronchoalveolar lavage fluid (BALF), comprising a diverse assortment of cellular and acellular components, serves as a direct proxy for airway secretions and is recognized as an optimal biological specimen for lung disease diagnostics.[23] In the present investigation, we initiated proteomic and metabolomic interrogations of BALF derived from patients at varying stages of CWP miners. Subsequently, these multiomics data sets were fused to discern the dynamics of disease progression in CWP, unveiling aberrant signaling cascades and promising therapeutic targets that could potentially be harnessed in future clinical endeavors to propel the advancement of precision medicine for lung disorders.

BALF comprises a variety of cellular and noncellular components, functioning as a direct equivalent to airway secretions. BALF effectively differentiates between infectious lung diseases, immune-related noninfectious diseases, and even malignant tumors, thus serving as a secure and efficient approach to investigate local immune pathological processes in the lungs.[23] Presently, BALF is employed for omics analysis in various lung disease studies.[24] In this research, we conducted proteomic and metabolomic analyses on BALF samples from patients with CWP across different stages, identifying protein, metabolite, and functional disparities among these patients. This provides valuable insights for early diagnosis and therapeutic intervention in CWP patients.

METHODS

Study Subjects

Between August and October 2023, we recruited underground workers from the Xishan Coal Mine in Taiyuan, focusing exclusively on roadway excavation workers due to the elevated dust production, exposure concentrations, and associated health risks. Ultimately, 18 participants were enrolled, comprising 6 coal miners and 12 coal workers with pneumoconiosis (CWPs), all fulfilling the Chinese GBZ 70−2015 diagnostic criteria. All participants were male. The CWPs were categorized into stages I (6 cases), II (4 cases), and III (2 cases) based on radiographic findings. Given the limited stage III cases, we established three groups: the no pneumoconiosis group (coal miners, CM), early pneumoconiosis group (stage I CWP, IC), and pneumoconiosis progression group (nonstage I CWP, NIC). The study adhered to ethical guidelines, with written informed consent obtained from all participants, in accordance with the Declaration of Helsinki. Participants completed questionnaires, clinical lab tests, X-rays, and pulmonary function tests. Collect bronchoalveolar lavage fluid from all participants for proteomic and metabolomic analysis. This study was approved by the Ethics Committee of the First Hospital of Shanxi Medical University (2020 K−K NO. 104) and obtained informed consent from each participant.

Inclusion Criteria for CWP.

Male participants aged over 40 years.

A history of exposure to coal dust exceeding 10 years, accompanied by a confirmed diagnosis of coal workers' pneumoconiosis.

Exclusion Criteria for CWP.

Presence of other significant respiratory conditions, including tuberculosis, lung cancer, and various interstitial lung diseases.

Coexisting illnesses such as heart failure, hepatic fibrosis, renal fibrosis, or other related fibrotic disorders.

History of other systemic malignant tumors or prior radiotherapy.

Inclusion Criteria for Coal Miners.

Male participants aged over 40 years.

A history of exposure to coal dust for more than 10 years, without a diagnosis of CWP.

Exclusion criteria for coal miners are identical to those for CWP.

BALF Collection and Processing

Local anesthesia was administered to the lung segments scheduled for BALF, and 1−2 mL of 2% lidocaine was injected through the biopsy channel. After securely positioning the electronic bronchoscope in the middle lobe of the right lung, 100 mL of sterile saline at 37 °C was instilled through the biopsy channel in divided doses of 20−30 mL each. The irrigation fluid was recovered by suction at a negative pressure of less than −100 mmHg, with a recovery rate exceeding 30% (total volume not less than 30 mL). The recovered solution was gently agitated, filtered through four layers of sterile gauze to remove mucus, centrifuged at 4000 rpm for 10 min, and the supernatant was immediately removed and stored in a −80 °C freezer.

Proteomics

Proteomic data analysis was conducted by Nanjing Personalbio Gene Technology Company. SDT buffer (comprising 4% SDS and 100 mM Tris-HCl at pH 7.6) was utilized for the lysis of BALF samples and subsequent protein extraction. Protein digestion was carried out adhering to the FASP protocol.[25] The resulting digested peptides underwent desalting on a C18 chromatographic column (Empore SPE Cartridges, standard density, with an internal diameter of 7 mm and a volume of 3 mL, Sigma). Following desalting, the peptides were concentrated via vacuum centrifugation and reconstituted in 40 μL of 0.1% (v/v) formic acid solution. The peptide concentration

https://doi.org/10.1021/acs.jproteome.4c00715
J. Proteome Res. 2025, 24, 1715−1731

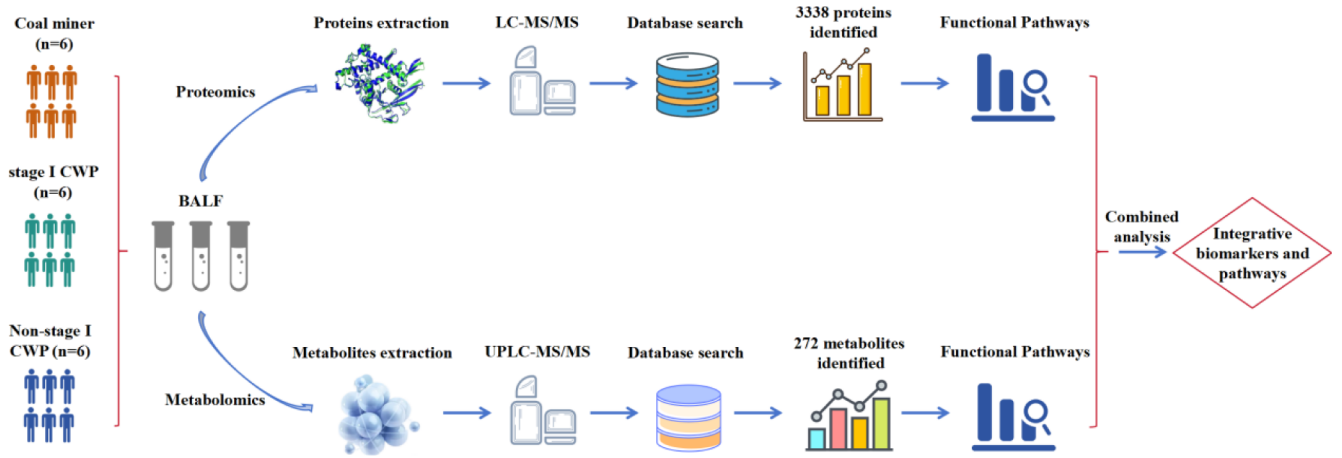

Figure 1. Summary of the study design. This clinical study recruited 18 participants, comprising six coal miners without pneumoconiosis, six patients with stage I coal worker's pneumoconiosis, and six patients with nonstage I coal worker's pneumoconiosis. Bronchoalveolar lavage fluid was collected from all participants for subsequent proteomic and metabolomic analyses. Specifically, the coal miners served as the control group without pneumoconiosis, the patients with stage I coal worker's pneumoconiosis represented the early stage of the disease, and the patients with nonstage I coal worker's pneumoconiosis denoted the progression stage of the disease.

was estimated by measuring the UV spectral density at 280 nm, utilizing an extinction coefficient of 1.1 for a 0.1% (g/l) solution.

LC-MS/MS analysis was performed on the timsTOF Pro mass spectrometer coupled with Nanoelute. The peptides were loaded onto a C18-reversed phase analytical column (Thermo Scientific Easy Column, 25 cm in length, 75 μm inner diameter, packed with 1.9 μm resin) and dissolved in 95% buffer A (consisting of 0.1% formic acid solution). Separation was achieved using a linear gradient of buffer B (99.9% acetonitrile with 0.1% formic acid) at a flow rate of 300 nL/min. Data acquisition was conducted with positive ionization, applying an electrospray voltage of 1.5 kV. Precursors and fragments were analyzed by the TOF detector within a mass range of 100−1700 m/z. The timsTOF Pro was operated in parallel accumulation serial fragmentation (PASEF) mode, utilizing the following parameters: the ion mobility coefficient ($1/K_0$) was set between 0.6 and 1.6 Vs/cm^2, with 1 MS and 10 MS/MS PASEF scans. Active exclusion was enabled, with a release time of 24 s. The raw MS data were subsequently combined and searched using MaxQuant (version 1.6.14) for identification and quantification analysis. The qualitative and quantitative parameters of proteins are shown in Table S1. Additionally, this study utilized the UniProt and Homo_sapiens.GRCh38.pep.all.fasta databases. Results were filtered based on a false discovery rate (FDR) of ≤0.01 for proteins and peptides. Differentially expressed proteins (DEPs) were identified based on a fold change (FC) > 2 or FC < 0.5, with P < 0.05. Blast2Go software was used to perform GO enrichment analysis on all DEPs. The identified DEPs were imported into the KEGG database for functional pathway analysis.

Metabolomics

For nontargeted metabolomics analyses, data were acquired in both positive and negative ion modes utilizing an Ultrahigh Performance Liquid Chromatography-tandem Mass Spectrometry (UPLC-MS/MS) system, comprising a Thermo Vanquish liquid chromatography system (Thermo Fisher Scientific, USA) coupled with a Thermo Orbitrap Exploris 120 mass spectrometer (Thermo Fisher Scientific, USA). The operational parameters were set as follows: sheath gas pressure at 40 arbitrary units (arb), auxiliary gas flow at 10 arb, spray voltages of 3.50 kV and −2.50 kV for ESI(+) and ESI(−), respectively; capillary temperature maintained at 325 °C; MS1 scan range from m/z 100 to 1000; MS1 resolving power of 60,000 full width at half-maximum (fwhm); four data-dependent scans per cycle; MS/MS resolving power of 15,000 fwhm; normalized collision energy set to 30%; and dynamic exclusion time set to automatic.[26]

The MSConvert tool in the Proteowizard software package (v3.0.8789) was used to convert the raw mass spectrometry output files into mzXML file format. The R XCMS software package was employed for peak detection, peak filtering, and peak alignment. The parameters were set as follows: bw = 2, ppm = 15, peakwidth = c(5, 30), mzwid = 0.015, mzdiff = 0.01, and method = "centWave". Data normalization was achieved using total peak area normalization to eliminate systematic errors. The R package Ropls was used to perform principal component analysis (PCA), partial least-squares discriminant analysis (PLS-DA), and orthogonal partial least-squares discriminant analysis (OPLS-DA) for dimensionality reduction analysis. The permutation test method was used to perform overfitting testing on the model. P values were calculated based on statistical tests, variable importance in projection (VIP) was calculated using the OPLS-DA dimensionality reduction method, and FC was used to calculate the fold change between groups to measure the influence intensity and explanatory power of each metabolite content on sample classification discrimination, assisting in the screening of marker metabolites. Metabolites with significant differential expression (DEM) were identified based on VIP > 1.0, FC > 1 or FC < 1, and P < 0.05. MetaboAnalyst (www.metaboanalyst.ca) was used to perform KEGG pathway enrichment analysis on the DEMs. Calculate the P-value based on statistical tests, calculate the variable importance in projection (VIP) using the OPLS-DA dimensionality reduction method, and calculate the fold change (FC) to measure the influence intensity and explanatory power of each metabolite content on sample classification and discrimination, assisting in the screening of marker metabolites. Determine differentially expressed metabolites (DEMs) based on VIP > 1.0, FC > 1 or FC < 1, and P < 0.05. KEGG pathway enrichment analysis was performed on DEM using MetaboAnalyst (www.metaboanalyst.ca).

https://doi.org/10.1021/acs.jproteome.4c00715
J. Proteome Res. 2025, 24, 1715−1731

Table 1. Summary of Participant Characteristics[a]

Characteristic	CM	IC	NIC	P value
General information				
Age (years)	49.67 ± 1.86	49.67 ± 3.07	49.50 ± 5.20	0.996
BMI (kg/m^2)	24.55 ± 2.17	26.21 ± 2.19	24.38 ± 1.34	0.228
Systolic blood pressure (mmHg)	136.50 ± 12.85	143.00 ± 15.92	144.00 ± 4.24	0.509
Diastolic blood pressure (mmHg)	93.50 ± 6.25	101.40 ± 13.58	94.50 ± 14.98	0.528
Years of occupational exposure (years)	17.48 ±1.95	18.56 ± 2.55	16.02 ± 2.28	0.188
Routine full blood analysis				
WBC (×10^9/L)	4.866 ± 0.66	4.84 ± 1.33	7.033 ± 2.03	**0.035**
RBC (×10^{12}/L)	4.821 ± 0.29	4.948 ± 0.39	4.87 ± 0.35	0.833
HGB (g/L)	156.00 ± 7.12	156.00 ± 11.96	163.67 ± 6.71	0.253
PLT (×10^9/L)	245.33 ± 43.29	240.20 ± 31.28	235.67 ± 48.10	0.924
Pulmonary function				
FVC_%pred	100.72 ± 14.60	99.46 ± 10.78	101.16 ± 10.54	0.969
FEV1_%pred	97.11 ± 15.76	93.89 ± 8.94	87.67 ± 14.24	0.476
FEV1/FVC	78.70 ± 7.44	77.10 ± 5.49	71.53 ± 15.09	0.461
MMEF75/25_%pred	76.73 ± 21.31	68.58 ±17.27	53.72 ± 25.52	0.208
MEF50_%pred	84.72 ± 23.46	80.10 ± 20.15	58.73 ± 27.04	0.163
MEF25_%pred	64.84 ± 20.81	52.21 ± 14.27	49.71 ± 31.06	0.494
DLCO SB%	92.32 ± 9.72	92.48 ± 13.99	93.70 ± 23.57	0.988

[a]WBC: white blood cell count; RBC: red blood cell count; HGB: hemoglobin; PLT: platelet count. Bold values indicate significant differences.

Enzyme Linked Immunosorbent Assay (ELISA) Verification

BALF samples from subjects who underwent proteomic analysis in the early stage were selected for ELISA verification. Additionally, based on the inclusion and exclusion criteria used in the proteomic analysis, six coal miners and 14 patients outside the cohort were also selected for molecular level verification. The levels of FMOD, TFR, CSF1, and ABCD2 in BALF were verified using the ELISA method.

Statistical Analysis

Statistical analysis of the data was performed using SPSS version 22.0. All data were statistically described using mean ± standard deviation (SD). To evaluate the differences between two groups, we employed the t test. For comparisons among three groups, we utilized one-way analysis of variance (ANOVA) and least significant difference (LSD) test. $P < 0.05$ was considered statistically significant. To assess the relationship between differential proteins and metabolites, we adopted the Spearman correlation test. Statistical significance was determined when $P < 0.05$. A correlation coefficient $|r| > 0.8$ indicates a strong correlation.

RESULTS

Clinical Characteristics of Participants

In this prospective study, we selected the emblematic Xishan coal mine in Shanxi Province to mitigate the confounding effects of regional variations in coal quality. Employing a multiomics approach, we delved into the aberrant pathways implicated in the initiation and progression of CWP, alongside potential biomarkers. The study's design is illustrated in Figure 1. Adhering to the Chinese GBZ 70-2015 diagnostic criteria for pneumoconiosis, we enrolled three candidate groups: CM group, IC group, and NIC group, comprising a total of 18 male roadway excavation workers. Table 1 summarizes their demographic and clinical profiles.

The participants' ages spanned from 40 to 53 years, with BMI values ranging from 22.06 to 29.28 kg/m^2. Our analysis revealed no noteworthy disparities across groups in terms of baseline demographics, years of occupational exposure, RBC count, HGB levels, PLT count, or lung function parameters, underscoring the comparability and balance of the groups. Nevertheless, significant variations emerged in WBC levels among the three groups. In-depth analysis utilizing the least significant difference (LSD) t test confirmed statistically significant differences in WBC levels between the NIC group and both the CM and IC groups.

Proteomic Analysis

Proteomic experiments revealed that a total of 24,755 peptides were detected, with 22,648 unique peptides used for identification, resulting in the identification of 3,338 proteins (Table S2). Among them, 2,962 proteins were quantifiable. We identified a total of 3,170 overlapping proteins across the three groups. Compared to the CM group, 85 differentially expressed proteins were obtained in the IC group, including 59 down-regulated proteins and 26 up-regulated proteins (Table S3). In the NIC group, 114 differentially expressed proteins were obtained, including 75 down-regulated proteins and 39 up-regulated proteins (Table S4). Compared to the IC group, the NIC group obtained 37 differentially expressed proteins, including 20 down-regulated proteins and 17 up-regulated proteins (Figure 2A–C, Table S5). The distribution of differentially expressed proteins was analyzed through volcanic plots and cluster heatmaps (Figures 2D–F, S1A–C). For CM and IC, alterations were observed in the TGF-beta signaling pathway, PPAR signaling pathway, calcium signaling pathway, ferroptosis, cholesterol metabolism, and hematopoietic cell lineage. For CM and NIC, changes were noted in cell adhesion molecules, phagosome, Th1 and Th2 cell differentiation, efferocytosis, and autoimmune-related disease pathways. For IC and NIC, alterations were observed in the Hedgehog signaling pathway and ABC transporters pathway (Figure S1D–F).

In addition, the cluster heatmap also displayed the expression of 87 differentially expressed proteins among the three groups (Figure 3A). We also created box plots to illustrate the expression levels of four distinct proteins across three sample groups. Compared with the CM group, the levels of ADPGK, TFR, and HLA-A were significantly decreased in

https://doi.org/10.1021/acs.jproteome.4c00715
J. Proteome Res. 2025, 24, 1715−1731

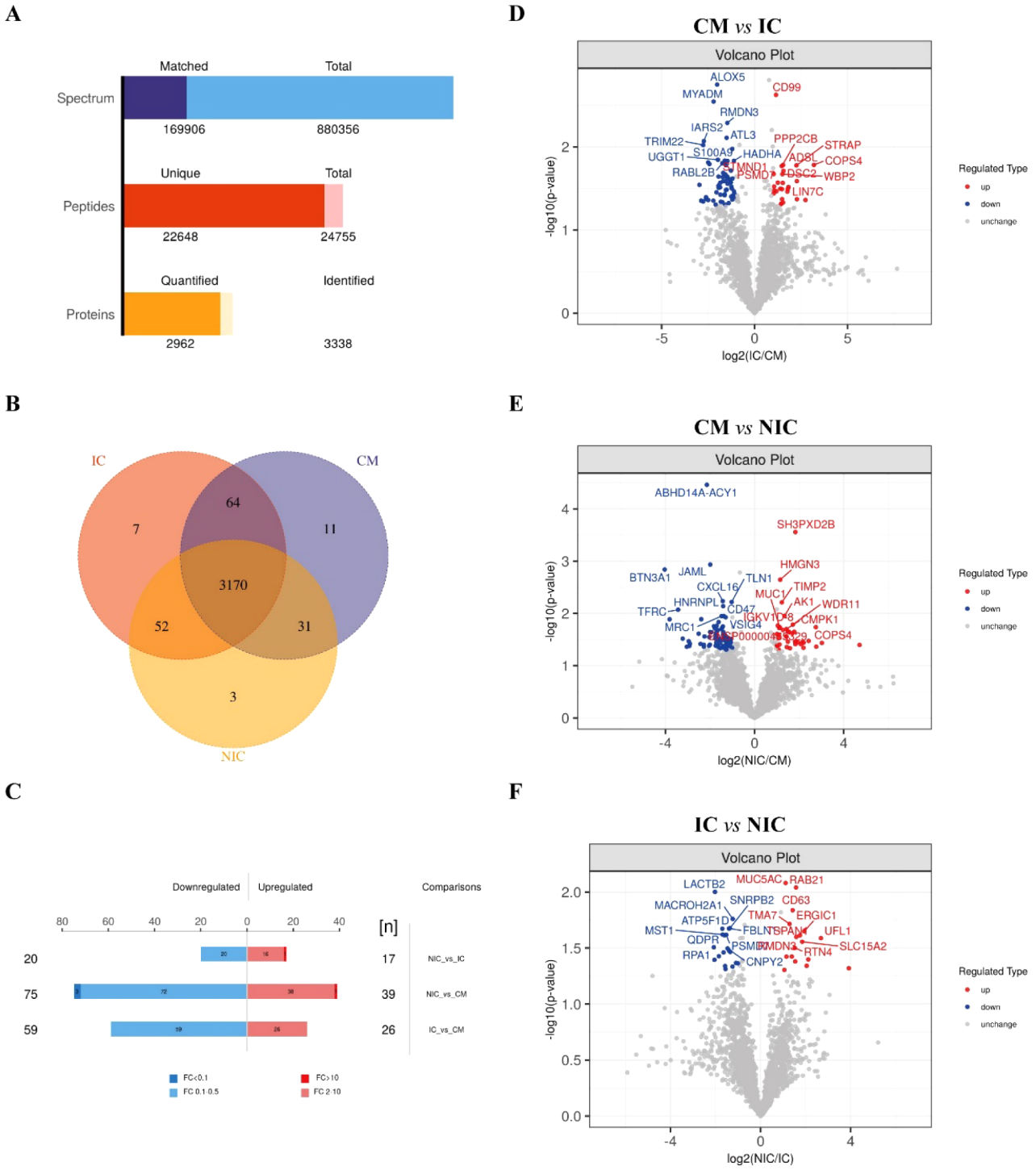

Figure 2. (A) Histogram illustrates identification and quantification results. (B) Venn diagram summarizes the differential and overlapping proteins. (C) Bar graph of protein quantification difference results. (D−F) The volcanic plot indicates significant changes in the proteins compared between the two groups.

both the IC group and NIC group, while the level of FMOD was significantly increased in the NIC group (Figure 3B-E).

GO enrichment and KEGG pathway analysis were conducted to further explore the functions associated with DEPs in the three groups. GO enrichment analysis revealed alterations in biological processes such as ATP hydrolysis coupled cation transmembrane transport and multicellular organism process (Figure S2A). Regarding GO molecular functions, in addition to calcium-transporting ATPase activity, ATPase activity coupled to transmembrane movement of ions, phosphorylative mechanism, cation-transporting ATPase activity, ATPase coupled ion transmembrane transporter activity, and active ion transmembrane transporter activity were also significantly enriched (Figure 4A). Furthermore, intrinsic component of membrane, integral component of membrane, and membrane cellular components may be related to these functions (Figure S2B). KEGG analysis indicated significant changes in pathways related to TGF-beta signaling pathway,

https://doi.org/10.1021/acs.jproteome.4c00715
J. Proteome Res. 2025, 24, 1715−1731

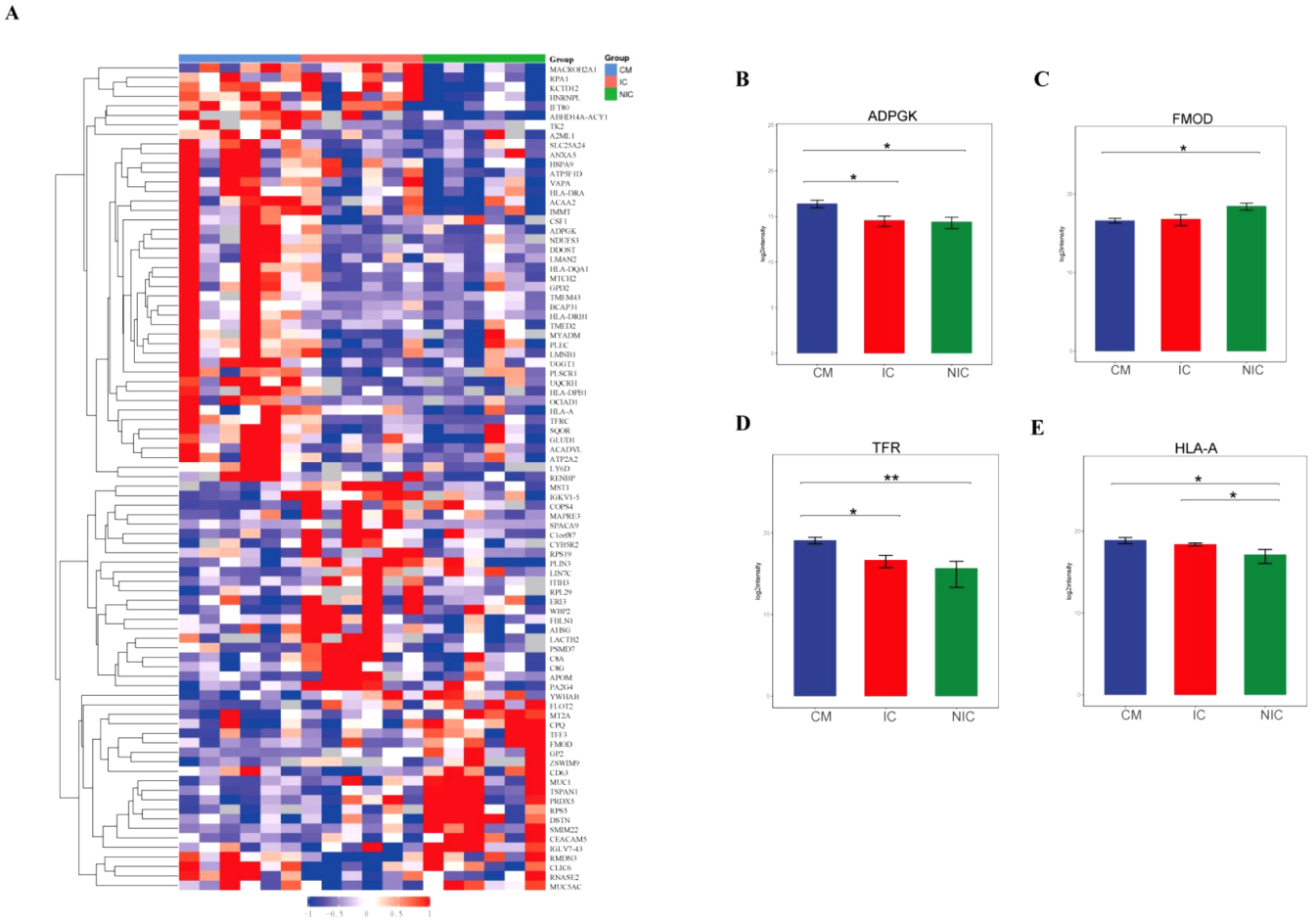

Figure 3. (A) The cluster heatmap illustrates the distribution of differentially expressed proteins among the three groups. The box plot of top performing proteins, including ADPGK (B), FMOD (C),TFR (D) and HLA-A (E). *P < 0.05, **P < 0.01.

arginine biosynthesis, hematopoietic cell lineage, and autoimmune-related diseases (Figure 4B).

Metabolomic Analysis

To further understand the metabolic changes in CWP patients, nontargeted metabolomics analysis was performed on BALF using the UHPLC-MS/MS system. The PLS-DA score plots showed clear separation of samples from the three groups in both positive and negative ion modes (Figure 5A,B). We further applied the OPLS-DA model to distinguish the metabolic characteristics of the three groups (positive ion mode: R2Y = 0.984 and Q2 = 0.676; negative ion mode: R2Y = 0.996 and Q2 = 0.627) (Figure 5C,D). Permutation tests confirmed the reliability of the model (Figure 5E,F).

This study identified 272 metabolites through database searching and comparative identification (Table S6). The volcanic plot and cluster heatmap revealed the distribution of differentially expressed metabolites between the two groups, showing a clear clustering of differentially expressed metabolites between the groups (Figures 6 and S3). Compared with the CM group, 24 metabolites were upregulated and 13 metabolites were downregulated in the IC group (Table S7); 19 metabolites were upregulated and 39 metabolites were downregulated in the NIC group (Table S8). Compared with the IC group, 19 metabolites were upregulated and 21 metabolites were downregulated in the NIC group (Table S9).

Subsequently, the box plot illustrated the significant upregulated and downregulated differential metabolites between the two groups of samples (Figure 7). The results indicated that, compared to the CM group, the L-methionine level in the IC group was notably downregulated, while the linoleic acid and urocanic acid levels were significantly upregulated. In the NIC group, both L-methionine and L-proline levels were significantly downregulated, while the oleic acid level was notably upregulated (P < 0.05). Compared to the IC group, the oleic acid and *S*-adenosylmethionine levels in the NIC group were significantly upregulated, while the S-hexylglutathione level was downregulated (P < 0.05).

In the analysis of metabolic pathways, we observed alterations in the metabolic pathways of pyrimidine metabolism, histidine metabolism, vitamin digestion and absorption, and protein digestion and absorption when comparing the CM group to the IC group. Comparing the CM group to the NIC group, changes were observed in the pathways of ABC transporters, protein digestion and absorption, aminoacyl-tRNA biosynthesis, central carbon metabolism in cancer, and mineral absorption. Furthermore, comparing the IC group to the NIC group, alterations were noted in the pathways of ABC transporters, Th17 cell differentiation, cysteine and methionine metabolism, as well as autoimmune-related diseases (Figures 8 and S4).

Integration of Proteomic and Metabolomic Analyses

The integrated analysis of proteomics and metabolomics revealed the common enrichment pathways of differential proteins and metabolites. In CM and IC, the common

https://doi.org/10.1021/acs.jproteome.4c00715
J. Proteome Res. 2025, 24, 1715−1731

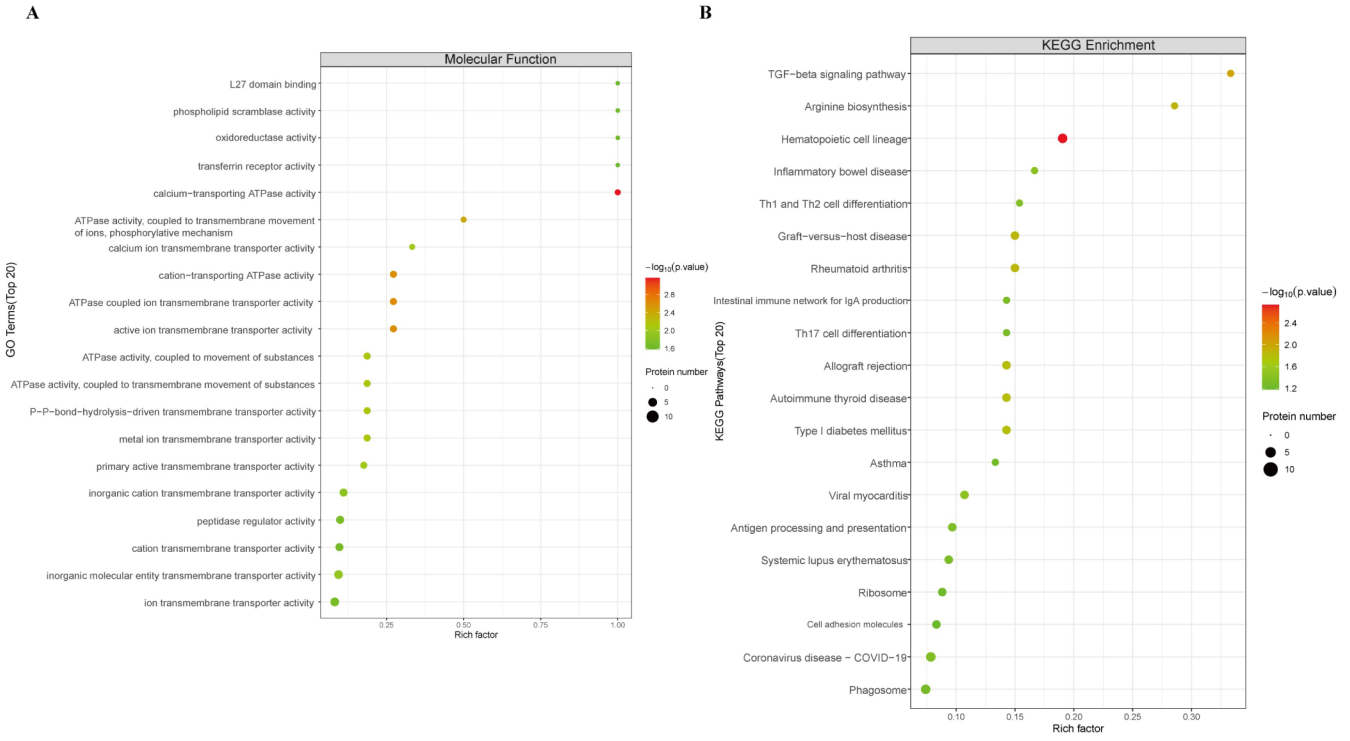

Figure 4. (A) Bubble chart of GO functional enrichment under molecular function classification across three group comparisons. (B) Perform KEGG functional analysis on the differentially expressed proteins among the three groups.

enrichment pathways include ABC transporters, aminoacyl-tRNA biosynthesis, folate biosynthesis, glutathione metabolism, HIF−1 signaling pathway, purine metabolism, and pyrimidine metabolism. In CM and NIC, the common enriched pathways include ABC transporters, amino sugar and nucleotide sugar metabolism, arachidonic acid metabolism, arginine biosynthesis, autophagy-animal, endocytosis, fatty acid degradation, Parkinson disease, purine metabolism, Rap1 signaling pathway, rheumatoid arthritis, shigellosis, thiamine metabolism, and valine, leucine, and isoleucine degradation. In IC and NIC, the common enrichment pathways include ABC transporters, folate biosynthesis, and pathways in cancer. We observed that the pathway of ABC transporters is common in CM and IC, CM and NIC, and IC and NIC (Figure 9A-C).

Based on the differences in proteins and metabolites in BALF of CWP patients at different stages, we further explored the correlation between differential proteins and differential metabolites. Spearman's correlation coefficient was used to determine the correlation. Notably, our results revealed a noteworthy association between changes in protein and metabolite profiles in CWP patients at different stages. Comparing CM with IC, CM with NIC, and IC with NIC, we observed a positive correlation between L-methionine and other proteins. For CM and NIC, oleic acid was positively correlated with PHPT1 and HMGN3. In the IC and NIC groups, oleic acid was positively correlated with RAB21 and ERGIC1. In the CM and IC group, (S)-beta-tyrosine was negatively correlated with ALOX5, whereas in the IC and NIC group, it was positively correlated with SF1 and MACRO-H2A1 (Figure 9D-F, Table S10).

In our data, the enrichment analysis results indicate that differentially expressed proteins are primarily enriched in the TGF-β signaling pathway and autoimmune disease-related signaling pathways. We observed that these pathways involve several important differentially expressed proteins, including TFR, FMOD, and CSF1 (Table S11). The ABC transporter pathway is a common pathway for differentially expressed proteins and metabolites across the three groups, and we found that ABCD2 is a key protein involved in the ABCD transporter pathway (Table S12).

To further validate the findings from proteomics, we utilized ELISA kits to verify differential proteins in independent samples. A summary of the characteristics of all independent samples with complete data is presented in Table S13. Consistent with the proteomic analysis experiment, compared to the CM group, FMOD expression level was upregulated in the NIC group. TFR level was consistently downregulated in both the IC and NIC groups. However, we did not observe significant differences in CSF1 protein expression in independent sample testing. Additionally, we assessed the expression of ABCD2, which is an important protein involved in the ABC transporter pathway, a commonly enriched pathway across the three groups in the integrated analysis. Consistent with the results of proteomic analysis, we observed that ABCD2 expression was upregulated in the IC group and downregulated in the NIC group (Figure 10).

DISCUSSION

CWP is a prevalent and severe occupational disease among coal miners, primarily caused by inhalation of mineral dust, leading to lung diseases. Currently, there is a lack of effective early diagnostic methods.[27] A deep understanding of the pathological characteristics of CWP is crucial for its diagnosis and intervention. Proteomics, as a powerful protein analysis method, can identify proteins involved in disease progression or therapeutic intervention as biomarkers.[28] In contrast, metabolomics technology can widely identify changes in small molecule metabolites, accurately reflecting the state of

https://doi.org/10.1021/acs.jproteome.4c00715
J. Proteome Res. 2025, 24, 1715−1731

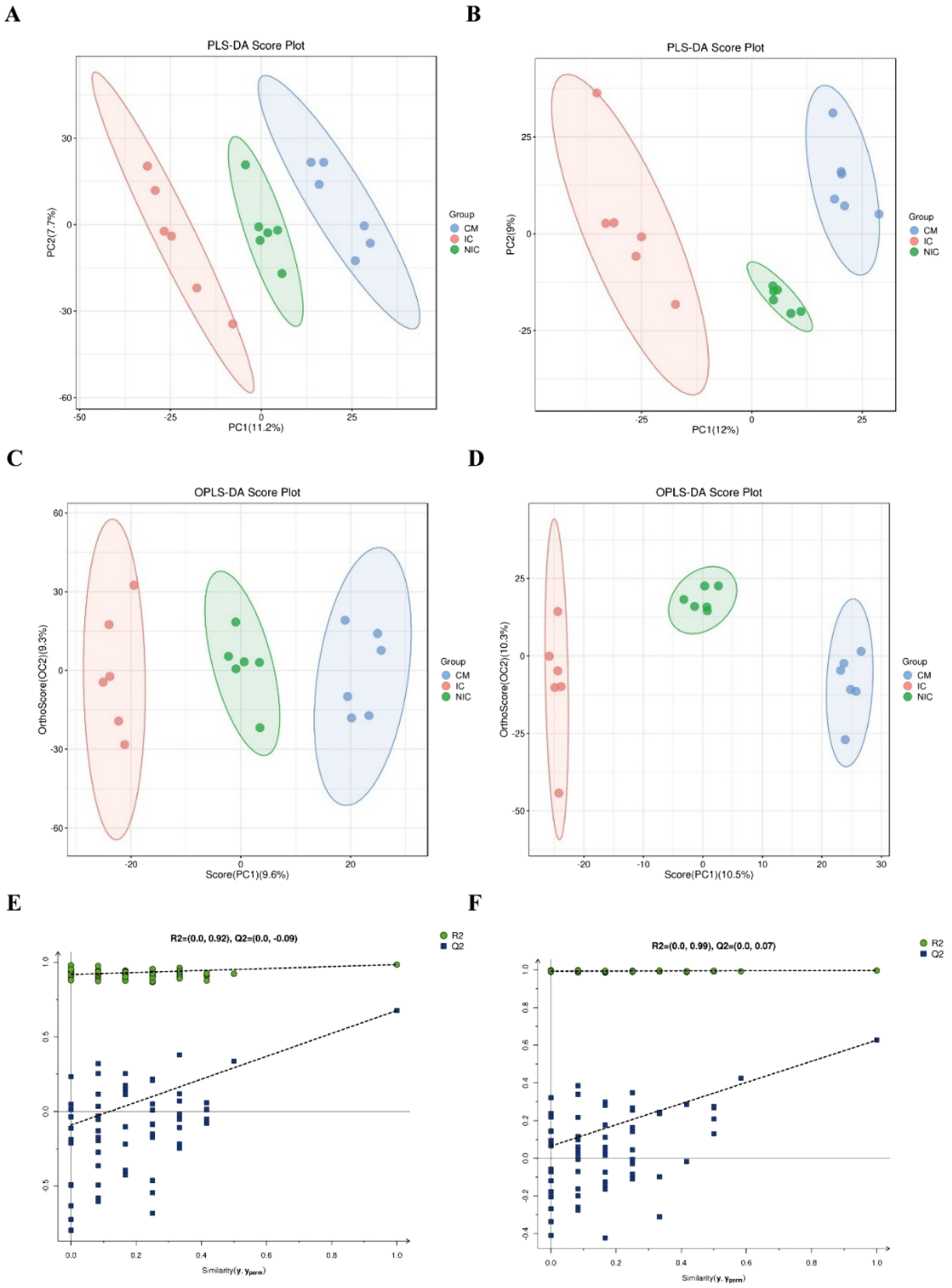

Figure 5. PCA score plots in (A) positive ion and (B) negative ion modes. OPLS-DA score plots in (C) positive ion and (D) negative ion modes. Permutation test plots under OPLS-DA for (E) positive ion and (F) negative ion modes.

biological systems.[29] Metabolite levels are also considered the ultimate response of biological systems to the occurrence and development of diseases.[30] Therefore, integrating proteomics and metabolomics analysis provides opportunities to address clinical issues related to CWP.[13] In this study, we integrated proteomic and metabolomic data from 18 healthy individuals,

https://doi.org/10.1021/acs.jproteome.4c00715
J. Proteome Res. 2025, 24, 1715−1731

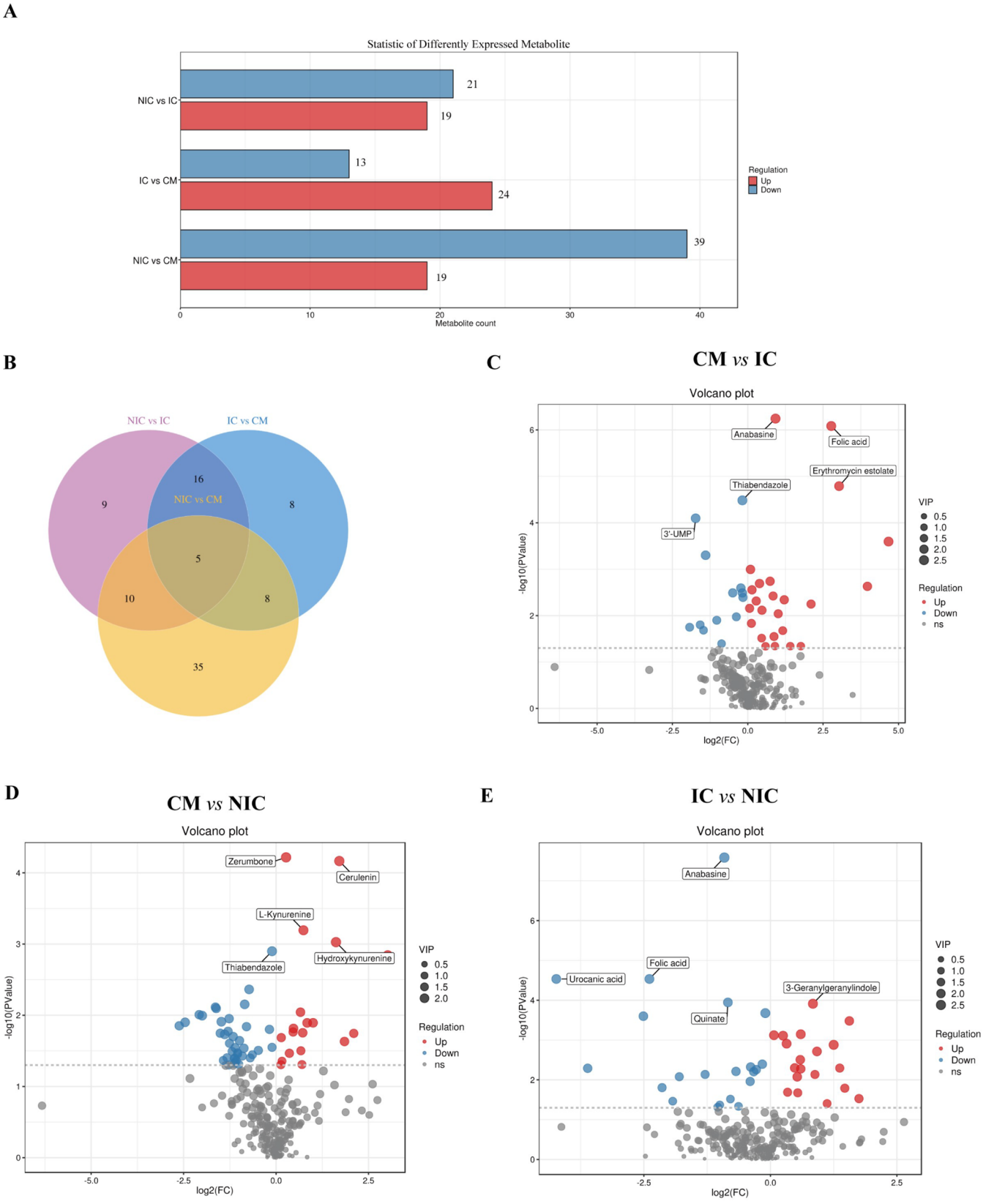

Figure 6. (A) Statistical histogram of differential metabolites. (B) Differential metabolite Venn diagram. (C–E) The volcano plot illustrates the variations in differential proteins between two groups.

early stage CWP patients, and advanced-stage CWP patients from the Xishan Coal Mine in Taiyuan. We focused on analyzing protein and metabolite profiles, as well as identifying DEPs and DEMs in BALF samples from patients with different stages of CWP. Additionally, this study further investigated key signaling pathways associated with these DEPs and DEMs. We

https://doi.org/10.1021/acs.jproteome.4c00715
J. Proteome Res. 2025, 24, 1715−1731

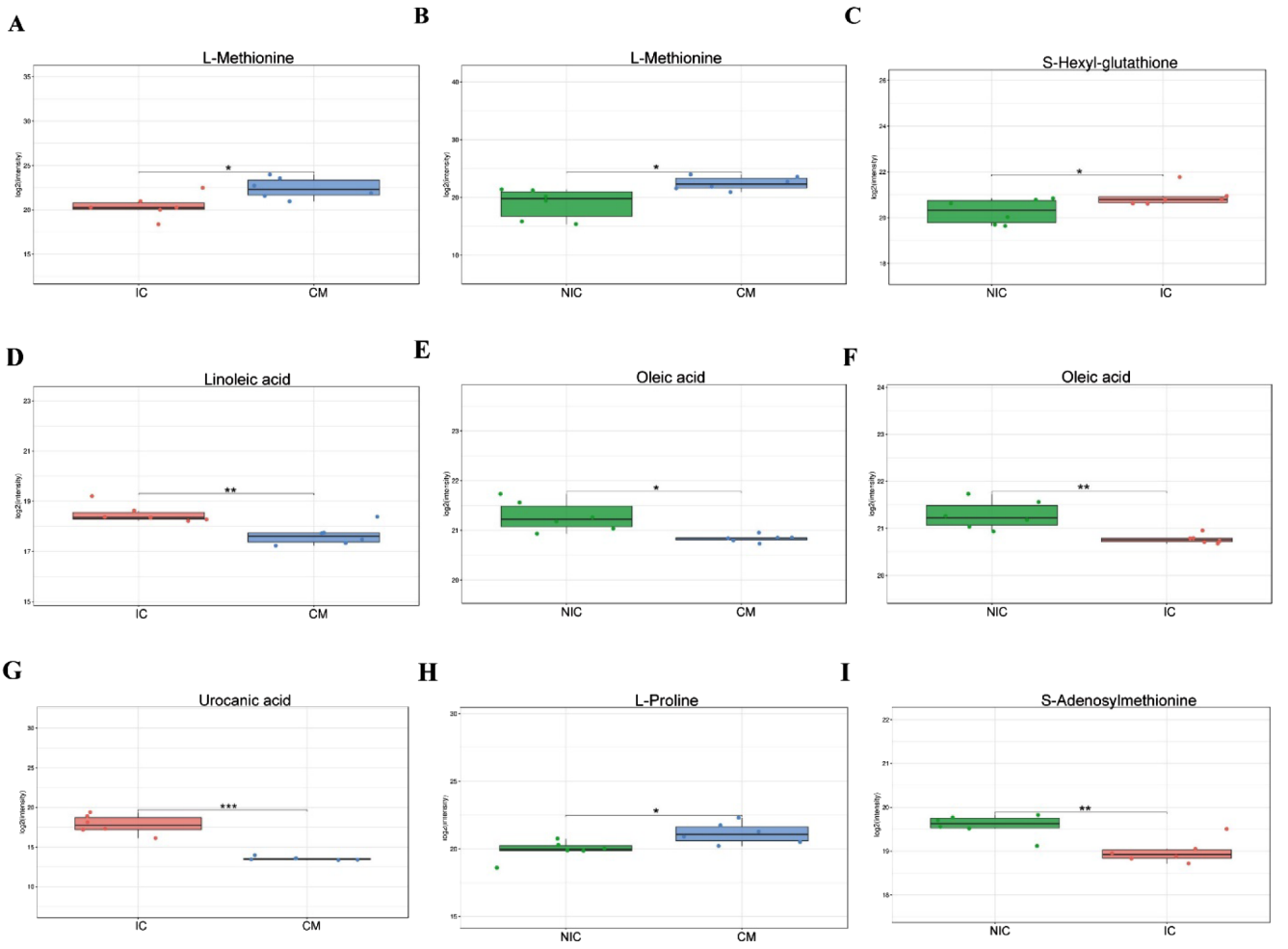

Figure 7. (A–I) The box plot illustrates the expression of differentially expressed metabolites that are upregulated and downregulated between the two groups. *$P < 0.05$, ** $P < 0.01$, ***$P < 0.001$.Blue represents the CM group, red represents the IC group, and green represents the NIC group.

found significant differences in the composition of protein and metabolite profiles among patients with different stages of CWP. We speculate that these differences may play an important role in the occurrence and development of CWP.

One of the main components of inhaled coal dust particles is silica. Silica can induce inflammatory cell infiltration, collagen fiber deposition, and abnormal repair of alveolar epithelial tissue by activating the inflammasome.[31−33] Therefore, the activation of the inflammasome caused by SiO_2 in inhaled dust is an important driving factor leading to pulmonary fibrosis. Through proteomics, this study found that compared with healthy coal miners, the ADPGK protein level was significantly reduced in the early CWP group and progressive CWP group. ADPGK is part of the glucose sensing system in the endoplasmic reticulum and plays a key role in regulating energy metabolism processes. The decrease in ADPGK will reduce glucose uptake by the body, decrease the activity of hexokinase, phosphofructokinase, and respiratory chain complexes, activate induced depletion of thymidine metabolic intermediates, and enhance autophagy, ultimately leading to energy metabolism disorders.[34] Some studies have pointed out that the activation of the inflammasome is related to energy metabolism disorders.[35] Therefore, the reason why inhaled coal dust particles promote pulmonary fibrosis by activating the inflammasome may be related to abnormal expression of ADPGK.

In addition to the abnormal expression level of ADPGK protein, this study also identified abnormalities in the expression levels of TFR and FMOD proteins through proteomics. The results of this study showed a significant decrease in TFR expression compared to the CM group. TFR is a type of integral membrane protein that mediates iron absorption through receptor-mediated endocytosis and is essential for maintaining intracellular iron homeostasis in cells.[36] Some studies have indicated that abnormalities in TFR expression in airway macrophages are involved in the formation of pulmonary fibrosis.[37] Under normal conditions, airway macrophages highly express TFR. However, in patients with pulmonary fibrosis, the expression of TFR in airway macrophages significantly decreases. The decrease in TFR expression in airway macrophages directly affects the phagocytic function of macrophages and promotes the development of a phenotype that promotes fibrosis. At the same time, an increase in the proportion of macrophages with low TFR expression is an independent risk factor for the survival time of patients with pulmonary fibrosis.[37] Combining our research results, it can be speculated that the decreased expression level of TFR in coal miners may be a risk factor for the development of CWP, and the potential mechanism may be related to the phenotypic changes of airway macrophages caused by the decreased expression level of TFR. At the same time, this study found a certain relationship between the

https://doi.org/10.1021/acs.jproteome.4c00715
J. Proteome Res. 2025, 24, 1715−1731

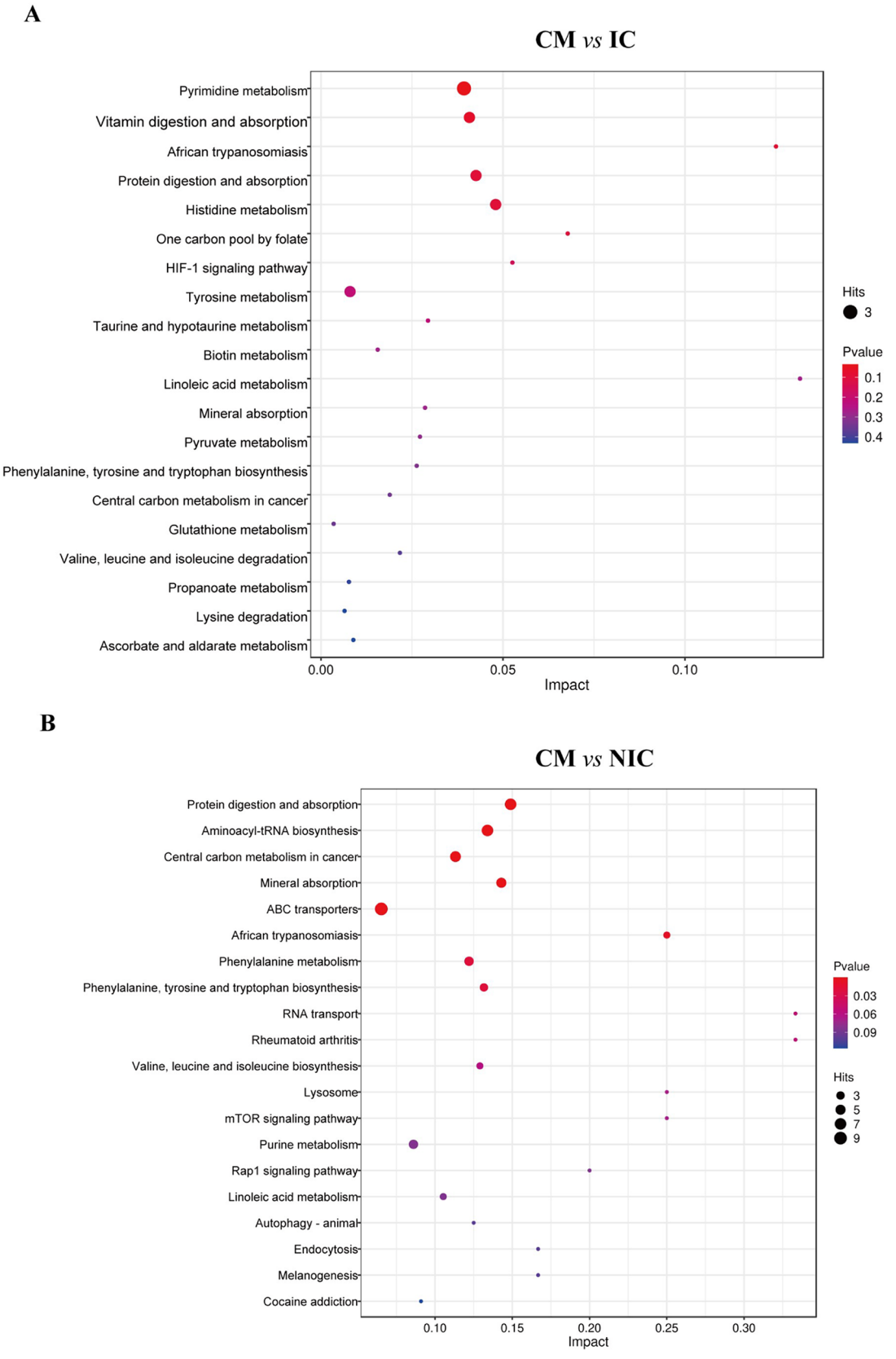

Figure 8. (A,B) Bubble chart of metabolic pathway influencing factors.

increase in FMOD levels and the progression of CWP. FMOD is a small leucine-rich proteoglycan (SLRP). Proteoglycans are important components of the extracellular matrix (ECM), widely distributed in connective tissues, and involved in regulating various cell growth and signal transduction processes in stromal tissues.[38−42] It is well-known that abnormal deposition of ECM is one of the important mechanisms underlying the occurrence of pulmonary fibrosis.

https://doi.org/10.1021/acs.jproteome.4c00715
J. Proteome Res. 2025, 24, 1715−1731

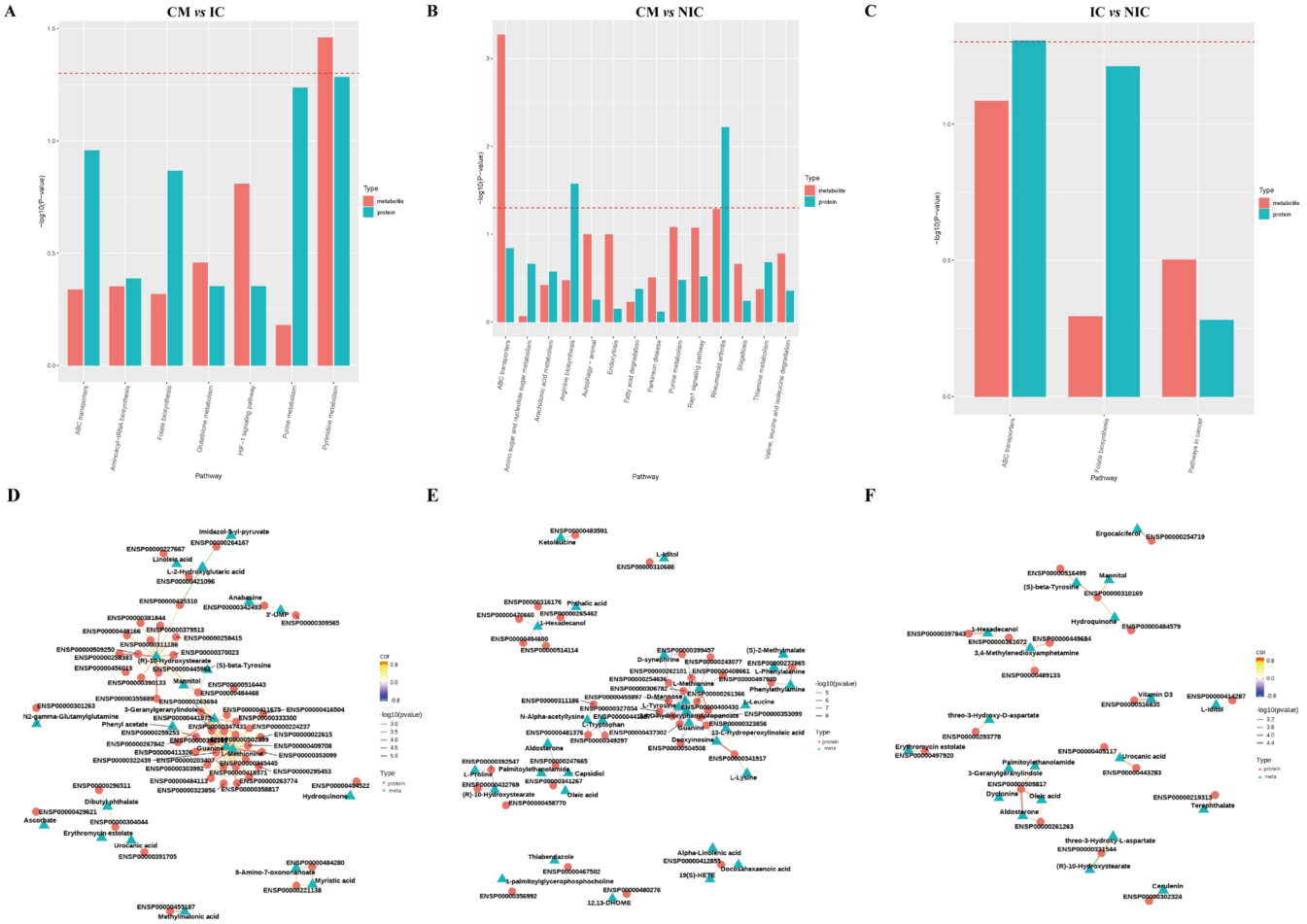

Figure 9. (A−C) Common enriched pathways of metabolome and proteome differences. The red dashed line indicates that *P* equals 0.05. Values above the red line are considered to have *P* less than 0.05. (D−F) Spearman correlation analysis of differential proteins and metabolites. Line colors represent correlation coefficients, line thickness indicates the significance level (*P* value), and node shapes distinguish between proteins and metabolites.

Previous studies on abnormal ECM deposition primarily focused on cells and substances traditionally highly associated with ECM formation and modification, such as fibroblasts, metalloproteinases, macrophages, alveolar epithelial cells, collagen, elastin, etc., neglecting the impact of FMOD on ECM and transforming growth factors.[43−47] Some studies have indicated that FMOD can promote fibrosis in patients with pancreatic and liver fibrosis by facilitating the deposition of collagen I and α-smooth muscle actin.[48,49] Therefore, the increased expression of FMOD in CWP patients may promote the formation of pulmonary fibrosis by regulating ECM formation. In summary, abnormalities in the expression levels of ADPGK, TFR, and FMOD may be involved in the formation and development of CWP, but further research is still needed.

In our data, the enrichment analysis results showed that the differentially expressed proteins were mainly enriched in the TGF-β signaling pathway and autoimmune disease-related signaling pathways. At the same time, we also discovered that the differentially expressed proteins TFR, FMOD, and CSF1 are all involved in these two signaling pathways. In mammals, there are three TGF-β isoforms with similar biological activities, including TGF-β1, TGF-β2, and TGF-β3.[50] Among them, TGF-β1 has the strongest effect on promoting tissue fibrosis.[51] Under normal conditions, TGF-β produced by cells exists in an inactive state. TGF-β and latency-associated peptide (LAP) are linked by disulfide bonds to form a dormant complex, which is cross-linked with the ECM. During the development of pulmonary fibrosis, the increased expression of integrin $\alpha v\beta 6$ on alveolar epithelial cells can help TGF-β remove LAP and become activated.[52,53] The promotion of pulmonary fibrosis by TGF-β mainly occurs through the following mechanisms: inducing apoptosis of alveolar epithelial cells, promoting ECM deposition, promoting fibroblast proliferation, inducing epithelial-mesenchymal transition, and synergizing with fibrogenic factors such as platelet-derived growth factor and connective tissue growth factor (CTGF).[54−58] The upregulation and fibrogenic role of TGF-β in the process of pulmonary fibrosis is an important basis for linking the TGF-β pathway with progressive pulmonary fibrosis in CWP patients. Meanwhile, the results of this study found that differentially expressed proteins were enriched in autoimmune-related disease signaling pathways. Some studies have pointed out that SiO_2 exposure can induce autoimmune disorders, which are related to changes in the function and number of T cells, including a decrease in the number of regulatory T cells, induction of $CD4^+$ T cell infiltration, and changes in $CD4^+$ T cell function.[59−62] In addition, some studies have pointed out that the use of PDL1-specific antibodies can block pulmonary fibrosis caused by $CD4^+$ T

https://doi.org/10.1021/acs.jproteome.4c00715
J. Proteome Res. 2025, 24, 1715−1731

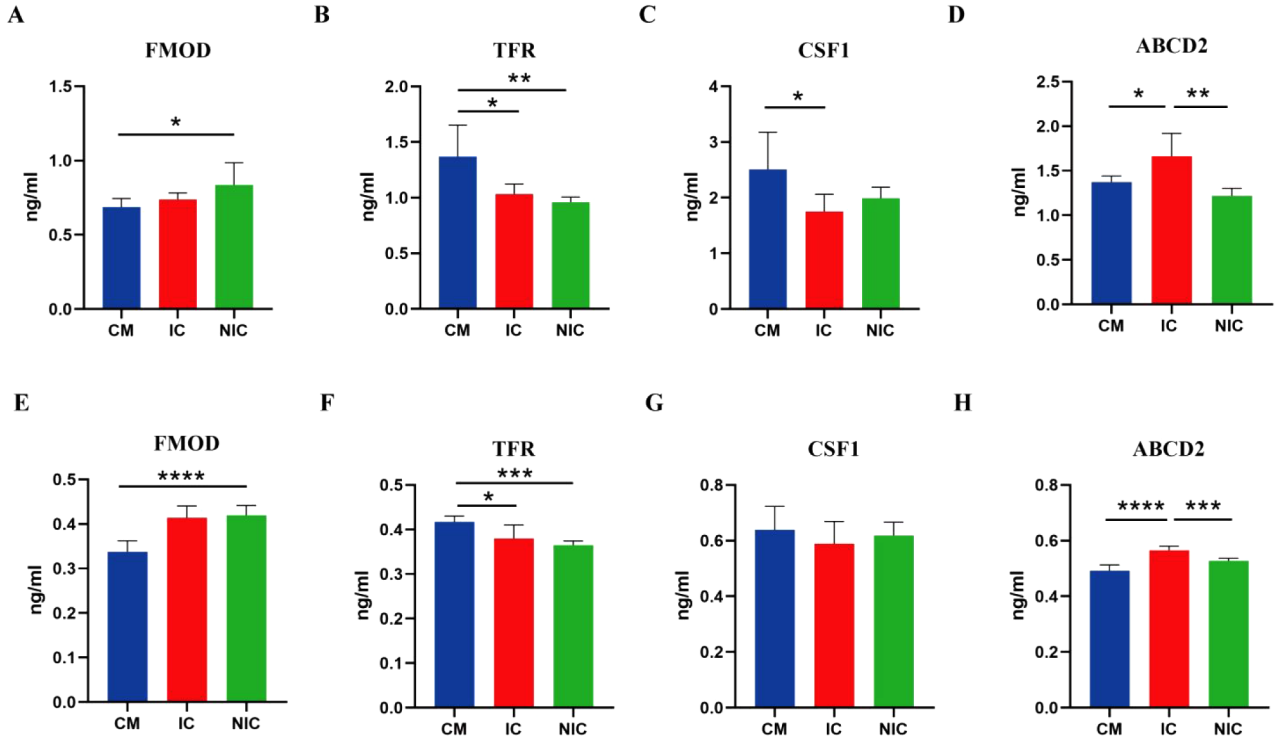

Figure 10. Content of differentially expressed proteins in the three groups of BALF was verified using the ELISA method. (A–D) ELISA detects the protein expression of subjects included in proteomic testing (n = 6). (E–H) ELISA detects the protein expression of independent subjects meeting the inclusion criteria (n = 6–7). *P < 0.05, ** P < 0.01, ***P < 0.001, ****P < 0.0001.

cell dysfunction.[63] Based on our research findings, it can be observed that CWP caused by coal mine dust may be associated with the activation of the TGF-β signaling pathway and T-cell dysfunction. Controlling the activation of the TGF-β signaling pathway through medication or correcting the dysfunction of T-cell subsets through immunotherapy may be the key to treating CWP.

Nontargeted metabolomics technology analyzed the metabolite profiles of CWP at different stages. Compared with the control group, 37 significantly different metabolites were identified in early CWP, and 58 differentially expressed metabolites were identified in progressive CWP. We observed that the levels of linoleic acid in the IC group and oleic acid in the NIC group were significantly increased compared to the CM group. Compared with the IC group, a significant increase in oleic acid was also observed in the NIC group. Linoleic acid and oleic acid belong to unsaturated fatty acids. It has been reported that linoleic acid metabolism plays a crucial role in the epithelial-mesenchymal transition induced by SiO_2 in human bronchial epithelial cells.[64] Oleic acid triggers intracellular pathways through different receptors, promoting the production of inflammatory factors and cell death.[65] Multiple studies have shown that oleic acid not only has direct toxicity to endothelial cells in the lungs, leading to cell necrosis and inducing capillary congestion and alveolar edema, but also activates caspase, promotes the production of reactive oxygen species, and induces mitochondrial depolarization and apoptosis in leukocytes.[66−70]

Furthermore, we also noticed changes in various amino acids and amino acid metabolic pathways in both the IC and NIC groups. This suggests that amino acid metabolic pathways may play a significant role in the progression of CWP. Compared to the CM group, we found that the urocanic acid level in the IC group was significantly elevated, and the histidine metabolic pathway underwent notable changes. In the histidine metabolic process, histidine is converted into urocanic acid, which is then converted into glutamic acid, and finally into glutathione, an antioxidant in the body. Studies have shown that under the stimulation of SiO_2, histidine metabolic imbalance disrupts bodily functions.[71] Compared to the CM group, the L-proline level in the NIC group was significantly reduced, and the protein digestion and absorption pathways underwent notable changes. The decrease in L-proline level may indicate a disorder in proline metabolism, which has been proven to be an important metabolic pathway in pulmonary fibrosis.[72,73] Additionally, comparisons between the IC and NIC groups, as well as among the three groups, revealed changes in the cysteine and methionine metabolic pathways. L-methionine, which participates in this pathway, was also found to be significantly reduced in the NIC group. Dysregulation of cysteine and methionine metabolism can seriously affect the body's glutathione levels and its ability to resist oxidative stress, which can undermine the body's anti-inflammatory and antioxidant capabilities.

After integrating and analyzing the data, we found that the common pathway involved in proteomics and metabolomics among the CM group and IC group, the CM group and NIC group, and the IC group and NIC group was ABC transporters pathway. Meanwhile, we found that ABCD2 is a key protein associated with the ABC transporter pathway. To validate our findings and further investigate the significance of identified proteins and metabolites, we selected TFR, FMOD, CSF1, and ABCD2 obtained from the bronchoalveolar lavage fluid in independent samples for further verification. The results confirmed that, consistent with proteomics experiments, compared to the CM group, the FMOD level was elevated

https://doi.org/10.1021/acs.jproteome.4c00715
J. Proteome Res. 2025, 24, 1715−1731

in the NIC group. The levels of TFR consistently decreased in both the IC and NIC groups. However, we did not observe significant differences in CSF1 protein expression in independent sample testing. Additionally, ABCD2 increased in the IC group but decreased in the NIC group. This corroborated the proteomic and metabolomic data. These findings suggest that these proteins may be closely associated with the progression of CWP.

ABC transporters represent a series of ATP-dependent membrane-integrated proteins, which are categorized into seven classes (ABCA, ABCB, ABCC, ABCD, ABDE, ABCF, and ABCG).[74,75] The main function of ABC transporters is to use the energy generated by ATP hydrolysis to transport substrates across membranes against concentration and gradient gradients.[76,77] ABC transporters transport a wide range of substrates, including sugars, amino acids, metal ions, peptides, proteins, cellular metabolites, etc.[76,78] The normal function and expression level of ABC transporters are crucial for the execution of normal physiological activities in cells. Studies have shown that the expression level of ABC transporters is relatively high in lung tissues.[79] Disruption of ABC transporter function can lead to lipid accumulation and elevated levels of inflammatory factors in lung tissues.[80] In addition, numerous studies have reported that multiple members of the ABC transporter family are involved in the occurrence and development of various lung diseases, including lung cancer, pulmonary alveolar proteinosis, and chronic obstructive pulmonary disease.[81−83] A decrease in the expression level of ABC transporters can affect the host's lung defense capabilities.[84,85] Currently, although the role of the ABC transporter protein family and ABCD2 in CWP has not been widely confirmed, the ABC transporter protein family has been proven to be capable of transporting various cytokines, ions, lipids, and detecting viral damage.[74,75] The expression of ABC transporter proteins in human airway epithelial cells may regulate the lung environment to respond to environmental exposures, including cigarette smoke, allergens, air pollution, bacteria, and viruses.[86]

Our study has some limitations. First, due to the small sample size, it is necessary to recruit more CWP patients in future studies to validate our results. Second, due to technical issues such as metabolite identification, some of the metabolites identified in this study do not originate from humans. Therefore, in future research, we need to expand our sample size and conduct in-depth exploration of the significant findings observed.

CONCLUSION

In our study, we discovered significant differences in proteins and metabolites present in the bronchoalveolar lavage fluid of CWP patients at various stages. In our proteomic analysis, we identified significant changes in the expression of proteins related to the TGF-β signaling pathway and autoimmune disease pathways in three groups, including TFR, FMOD, and CSF1. Integrated pathway analysis of proteins and metabolites in patients with CWP at different stages revealed alterations in the ABC transporter pathway, and further identified ABCD2 as a key protein involved in this pathway. Overall, this study identified metabolic characteristics in patients with CWP at different stages, aiming to reveal the underlying molecular mechanisms of CWP.

ASSOCIATED CONTENT

Data Availability Statement

The mass spectrometry proteomics data have been deposited to the ProteomeXchange Consortium (https://proteomecentral.proteomexchange.org/) via the PRIDE partner repository with the data set identifier PXD057353.

Supporting Information

The Supporting Information is available free of charge at https://pubs.acs.org/doi/10.1021/acs.jproteome.4c00715.

Figure S1: cluster heatmap and KEGG functional analysis of differential proteins between the two groups; Figure S2: GO enrichment analysis comparing among three groups; Figure S3: cluster heatmap analysis of differential metabolites between the two groups; Figure S4: Bubble chart of metabolic pathway influencing factors (PDF)

Table S1: proteomic analysis parameters (XLSX)

Table S2: protein identification list across three groups (XLSX)

Table S3: differential analysis of proteins in the comparison between IC and CM (XLSX)

Table S4: differential analysis of proteins in the comparison between NIC and CM (XLSX)

Table S5: differential analysis of proteins in the comparison between NIC and IC (XLSX)

Table S6: quantitative list of metabolites identified in the three groups (XLSX)

Table S7: differential analysis of metabolites in the comparison between IC and CM (XLSX)

Table S8: differential analysis of metabolites in the comparison between NIC and CM (XLSX)

Table S9: differential analysis of metabolites in the comparison between IC and NIC (XLSX)

Table S10: correlation analysis between differential proteins and metabolites (XLSX)

Table S11: pathway analysis of differentially expressed proteins observed in the comparison of three groups (XLSX)

Table S12: pathway analysis of differential proteins and metabolites (XLSX)

Table S13: characteristics of the independent samples (PDF)

AUTHOR INFORMATION

Corresponding Authors

Yiwei Shi − *Department of Respiratory and Critical Care Medicine, The First Hospital of Shanxi Medical University, Taiyuan, Shanxi 030001, China; NHC Key Laboratory of Pneumoconiosis, Taiyuan 030001, China*; Email: sdyysyw@163.com

Xiaomei Kong − *Department of Respiratory and Critical Care Medicine, The First Hospital of Shanxi Medical University, Taiyuan, Shanxi 030001, China; NHC Key Laboratory of Pneumoconiosis, Taiyuan 030001, China*; Email: sdyykxm@163.com

Min Pang − *Department of Respiratory and Critical Care Medicine, The First Hospital of Shanxi Medical University, Taiyuan, Shanxi 030001, China; NHC Key Laboratory of Pneumoconiosis, Taiyuan 030001, China*; Email: pangmin2009@126.com

Authors

Yangyang Wei − *Department of Respiratory and Critical Care Medicine, The First Hospital of Shanxi Medical University, Taiyuan, Shanxi 030001, China; NHC Key Laboratory of Pneumoconiosis, Taiyuan 030001, China*

Zhenzhen Jia − *Academy of Medical Sciences, Shanxi Medical University, Taiyuan, Shanxi 030001, China; NHC Key Laboratory of Pneumoconiosis, Taiyuan 030001, China;* orcid.org/0009-0008-8842-9421

Jing Ma − *Shanxi Cardiovascular Hospital, Taiyuan, Shanxi 030001, China*

Wei Zhang − *Department of Respiratory and Critical Care Medicine, The First Hospital of Shanxi Medical University, Taiyuan, Shanxi 030001, China; NHC Key Laboratory of Pneumoconiosis, Taiyuan 030001, China*

Hui Li − *Department of Respiratory and Critical Care Medicine, The First Hospital of Shanxi Medical University, Taiyuan, Shanxi 030001, China; NHC Key Laboratory of Pneumoconiosis, Taiyuan 030001, China*

Juan Wu − *Department of Respiratory and Critical Care Medicine, The First Hospital of Shanxi Medical University, Taiyuan, Shanxi 030001, China; NHC Key Laboratory of Pneumoconiosis, Taiyuan 030001, China*

Xiaojing Wang − *Department of Respiratory and Critical Care Medicine, The First Hospital of Shanxi Medical University, Taiyuan, Shanxi 030001, China; NHC Key Laboratory of Pneumoconiosis, Taiyuan 030001, China*

Xiao Yu − *Department of Respiratory and Critical Care Medicine, The First Hospital of Shanxi Medical University, Taiyuan, Shanxi 030001, China; NHC Key Laboratory of Pneumoconiosis, Taiyuan 030001, China*

Complete contact information is available at: https://pubs.acs.org/10.1021/acs.jproteome.4c00715

Author Contributions

M.P., X.M.K. and Y.Y.W. conceived the project. W.Z., J.W. and X.J.W. participated in the human sample collection. J.M., H.L., and X.Y. participated in the data collection and analyses. Y.Y.W. and Z.Z.J. wrote and revised the manuscript. M.P., X.M.K., and Y.W.S. edited the manuscript. All authors approved the final version for publication. M.P. and Y.Y.W. supervised the entire project.

Notes

The authors declare no competing financial interest.

■ ACKNOWLEDGMENTS

This project was funded by the Scientific and Technological Innovation Programs of Higher Education Institutions in Shanxi (grant number: 2022L139), the Fundamental Research Program of Shanxi Province (grant number: 202203021222370), and the Health Commission of Shanxi Province (grant number: 2023033). The authors thank the NHC Key Laboratory of Pneumoconiosis for its support.

■ REFERENCES

(1) Perret, J. L.; Plush, B.; Lachapelle, P.; Hinks, T. S. C.; Walter, C.; Clarke, P.; Irving, L.; Brady, P.; Dharmage, S. C.; Stewart, A. Coal Mine Dust Lung Disease in the Modern Era. *Respirology* **2017**, *22* (4), 662−670.

(2) Li, B.; Wang, J.; Zhao, Y.; Zou, Y.; Cao, H.; Jin, H.; Tao, X.; Mu, M. Vitamin D3 Reverses Immune Tolerance and Enhances the Cytotoxicity of Effector T Cells in Coal Pneumoconiosis. *Ecotoxicol. Environ. Saf.* **2024**, *271*, 115972.

(3) Hoy, R. F.; Chambers, D. C. Silica-Related Diseases in the Modern World. *Allergy* **2020**, *75* (11), 2805−2817.

(4) Leung, C. C.; Yu, I. T. S.; Chen, W. Silicosis. *Lancet* **2012**, *379* (9830), 2008−2018.

(5) Song, Y.; Southam, K.; Beamish, B. B.; Zosky, G. R. Effects of Chemical Composition on the Lung Cell Response to Coal Particles: Implications for Coal Workers' Pneumoconiosis. *Respirology* **2022**, *27* (6), 447−454.

(6) Yong, M. Comment on Tomaskova et al. Mortality in Miners with Coal-Workers' Pneumoconiosis in the Czech Republic in the Period 1992−2013. *Int. J. Environ. Res. Public Health*, 2017, 14, 269. *Int. J. Environ. Res. Public Health* **2018**, *15* (2), 276.

(7) Paul, R.; Adeyemi, O.; Arif, A. A. Estimating Mortality from Coal Workers' Pneumoconiosis among Medicare Beneficiaries with Pneumoconiosis Using Binary Regressions for Spatially Sparse Data. *Am. J. Ind. Med.* **2022**, *65* (4), 262−267.

(8) Mandrioli, D.; Schlünssen, V.; Ádám, B.; Cohen, R. A.; Colosio, C.; Chen, W.; Fischer, A.; Godderis, L.; Göen, T.; Ivanov, I. D.; Leppink, N.; Mandic-Rajcevic, S.; Masci, F.; Nemery, B.; Pega, F.; Prüss-Üstün, A.; Sgargi, D.; Ujita, Y.; van der Mierden, S.; Zungu, M.; Scheepers, P. T. J. WHO/ILO Work-Related Burden of Disease and Injury: Protocol for Systematic Reviews of Occupational Exposure to Dusts and/or Fibres and of the Effect of Occupational Exposure to Dusts and/or Fibres on Pneumoconiosis. *Environ. Int.* **2018**, *119*, 174−185.

(9) Yao, Y.; Wei, T.; Zhang, H.; Xie, Y.; Gu, P.; Yao, Y.; Xiong, X.; Peng, Z.; Zhen, Z.; Liu, S.; Cui, X.; Mei, L.; Ma, J. Characteristics of Diagnosed and Death Cases of Pneumoconiosis in Hubei Province, China, 1949−2019. *Int. J. Environ. Res. Public Health* **2022**, *19* (23), 15799.

(10) Binay, S.; Arbak, P.; Safak, A. A.; Balbay, E. G.; Bilgin, C.; Karatas, N. Does Periodic Lung Screening of Films Meets Standards? *Pak. J. Med. Sci.* **2016**, *32* (6), 1506−1511.

(11) McCall, C. The Cost of Complacency-Black Lung in Australia. *Lancet* **2017**, *390* (10096), 727−729.

(12) Blackley, D. J.; Halldin, C. N.; Cummings, K. J.; Laney, A. S. Lung Transplantation Is Increasingly Common among Patients with Coal Workers' Pneumoconiosis. *Am. J. Ind. Med.* **2016**, *59* (3), 175−177.

(13) Qi, X.-M.; Luo, Y.; Song, M.-Y.; Liu, Y.; Shu, T.; Liu, Y.; Pang, J.-L.; Wang, J.; Wang, C. Pneumoconiosis: Current Status and Future Prospects. *Chin Med. J. (Engl.)* **2021**, *134* (8), 898−907.

(14) Wang, W.; Jia, H.-L.; Huang, J.-M.; Liang, Y.-C.; Tan, H.; Geng, H.-Z.; Guo, L.-Y.; Yao, S.-Z. Identification of Biomarkers for Lymph Node Metastasis in Early-Stage Cervical Cancer by Tissue-Based Proteomics. *Br. J. Cancer* **2014**, *110* (7), 1748−1758.

(15) An, R.; Yu, H.; Wang, Y.; Lu, J.; Gao, Y.; Xie, X.; Zhang, J. Integrative Analysis of Plasma Metabolomics and Proteomics Reveals the Metabolic Landscape of Breast Cancer. *Cancer Metab.* **2022**, *10* (1), 13.

(16) Qian, Y.; Tong, Y.; Zeng, Y.; Huang, J.; Liu, K.; Xie, Y.; Chen, J.; Gao, M.; Liu, L.; Zhao, J.; Hong, Y.; Nie, X. Integrated Lipid Metabolomics and Proteomics Analysis Reveal the Pathogenesis of Polycystic Ovary Syndrome. *J. Transl. Med.* **2024**, *22* (1), 364.

(17) Evans, C. R.; Karnovsky, A.; Kovach, M. A.; Standiford, T. J.; Burant, C. F.; Stringer, K. A. Untargeted LC-MS Metabolomics of Bronchoalveolar Lavage Fluid Differentiates Acute Respiratory Distress Syndrome from Health. *J. Proteome Res.* **2014**, *13* (2), 640−649.

(18) Kan, M.; Shumyatcher, M.; Himes, B. E. Using Omics Approaches to Understand Pulmonary Diseases. *Respir. Res.* **2017**, *18* (1), 149.

(19) Karczewski, K. J.; Snyder, M. P. Integrative Omics for Health and Disease. *Nat. Rev. Genet.* **2018**, *19* (5), 299−310.

(20) Nalbantoglu, S.; Karadag, A. Metabolomics Bridging Proteomics along Metabolites/Oncometabolites and Protein Mod-

ifications: Paving the Way toward Integrative Multiomics. *J. Pharm. Biomed. Anal.* **2021**, *199*, 114031.
(21) Larina, I. M.; Ivanisenko, V. A.; Nikolaev, E. N.; Grigorev, A. I. The Proteome of a Healthy Human during Physical Activity under Extreme Conditions. *Acta Nat.* **2014**, *6* (3), 66−75.
(22) Chen, Z.-Z.; Gerszten, R. E. Metabolomics and Proteomics in Type 2 Diabetes. *Circ. Res.* **2020**, *126* (11), 1613.
(23) Jacobs, J. A.; Stobberingh, E. E.; Cornelissen, E. I. M.; Drent, M. Detection of Streptococcus Pneumoniae Antigen in Bronchoalveolar Lavage Fluid Samples by a Rapid Immunochromatographic Membrane Assay. *J. Clin. Microbiol.* **2005**, *43* (8), 4037−4040.
(24) Kruk, M. E.; Mehta, S.; Murray, K.; Higgins, L.; Do, K.; Johnson, J. E.; Wagner, R.; Wendt, C. H.; O'Connor, J. B.; Harris, J. K.; Laguna, T. A.; Jagtap, P. D.; Griffin, T. J. An Integrated Metaproteomics Workflow for Studying Host-Microbe Dynamics in Bronchoalveolar Lavage Samples Applied to Cystic Fibrosis Disease. *mSystems* **2024**, *9* (7), No. e0092923.
(25) Wiśniewski, J. R.; Zougman, A.; Nagaraj, N.; Mann, M. Universal Sample Preparation Method for Proteome Analysis. *Nat. Methods* **2009**, *6* (5), 359−362.
(26) Want, E. J.; Masson, P.; Michopoulos, F.; Wilson, I. D.; Theodoridis, G.; Plumb, R. S.; Shockcor, J.; Loftus, N.; Holmes, E.; Nicholson, J. K. Global Metabolic Profiling of Animal and Human Tissues via UPLC-MS. *Nat. Protoc.* **2013**, *8* (1), 17−32.
(27) Zhang, N.; Liu, K.; Wang, K.; Zhou, C.; Wang, H.; Che, S.; Liu, Z.; Yang, H. Dust Induces Lung Fibrosis through Dysregulated DNA Methylation. *Environ. Toxicol.* **2019**, *34* (6), 728−741.
(28) Angel, T. E.; Aryal, U. K.; Hengel, S. M.; Baker, E. S.; Kelly, R. T.; Robinson, E. W.; Smith, R. D. Mass Spectrometry-Based Proteomics: Existing Capabilities and Future Directions. *Chem. Soc. Rev.* **2012**, *41* (10), 3912−3928.
(29) Clish, C. B. Metabolomics: An Emerging but Powerful Tool for Precision Medicine. *Cold Spring Harbor Mol. Case Stud.* **2015**, *1* (1), a000588.
(30) Fiehn, O. Metabolomics–the Link between Genotypes and Phenotypes. *Plant Mol. Biol.* **2002**, *48* (1−2), 155−171.
(31) Cassel, S. L.; Eisenbarth, S. C.; Iyer, S. S.; Sadler, J. J.; Colegio, O. R.; Tephly, L. A.; Carter, A. B.; Rothman, P. B.; Flavell, R. A.; Sutterwala, F. S. The Nalp3 Inflammasome Is Essential for the Development of Silicosis. *Proc. Natl. Acad. Sci. U. S. A.* **2008**, *105* (26), 9035−9040.
(32) Dostert, C.; Pétrilli, V.; Van Bruggen, R.; Steele, C.; Mossman, B. T.; Tschopp, J. Innate Immune Activation through Nalp3 Inflammasome Sensing of Asbestos and Silica. *Science* **2008**, *320* (5876), 674−677.
(33) Peeters, P. M.; Perkins, T. N.; Wouters, E. F. M.; Mossman, B. T.; Reynaert, N. L. Silica Induces NLRP3 Inflammasome Activation in Human Lung Epithelial Cells. *Part. Fibre Toxicol.* **2013**, *10*, 3.
(34) Imle, R.; Wang, B.-T.; Stützenberger, N.; Birkenhagen, J.; Tandon, A.; Carl, M.; Himmelreich, N.; Thiel, C.; Gröne, H.-J.; Poschet, G.; Völkers, M.; Gülow, K.; Schröder, A.; Carillo, S.; Mittermayr, S.; Bones, J.; Kamiński, M. M.; Kölker, S.; Sauer, S. W. ADP-Dependent Glucokinase Regulates Energy Metabolism via ER-Localized Glucose Sensing. *Sci. Rep.* **2019**, *9* (1), 14248.
(35) Brandes, R. P.; Rezende, F. Glycolysis and Inflammation: Partners in Crime! *Circ. Res.* **2021**, *129* (1), 30−32.
(36) Kawabata, H. Transferrin and Transferrin Receptors Update. *Free Radical Biol. Med.* **2019**, *133*, 46−54.
(37) Allden, S. J.; Ogger, P. P.; Ghai, P.; McErlean, P.; Hewitt, R.; Toshner, R.; Walker, S. A.; Saunders, P.; Kingston, S.; Molyneaux, P. L.; Maher, T. M.; Lloyd, C. M.; Byrne, A. J. The Transferrin Receptor CD71 Delineates Functionally Distinct Airway Macrophage Subsets during Idiopathic Pulmonary Fibrosis. *Am. J. Respir. Crit. Care Med.* **2019**, *200* (2), 209−219.
(38) Iozzo, R. V.; Schaefer, L. Proteoglycan Form and Function: A Comprehensive Nomenclature of Proteoglycans. *Matrix Biol.* **2015**, *42*, 11−55.
(39) Nikitovic, D.; Aggelidakis, J.; Young, M. F.; Iozzo, R. V.; Karamanos, N. K.; Tzanakakis, G. N. The Biology of Small Leucine-Rich Proteoglycans in Bone Pathophysiology. *J. Biol. Chem.* **2012**, *287* (41), 33926−33933.
(40) Pang, X.; Dong, N.; Zheng, Z. Small Leucine-Rich Proteoglycans in Skin Wound Healing. *Front. Pharmacol.* **2020**, *10*, 1649.
(41) Schaefer, L.; Iozzo, R. V. Biological Functions of the Small Leucine-Rich Proteoglycans: From Genetics to Signal Transduction. *J. Biol. Chem.* **2008**, *283* (31), 21305−21309.
(42) Zheng, Z.; Li, C.; Ha, P.; Chang, G. X.; Yang, P.; Zhang, X.; Kim, J. K.; Jiang, W.; Pang, X.; Berthiaume, E. A.; Mills, Z.; Haveles, C. S.; Chen, E.; Ting, K.; Soo, C. CDKN2B Upregulation Prevents Teratoma Formation in Multipotent Fibromodulin-Reprogrammed Cells. *J. Clin. Invest.* **2019**, *129* (8), 3236−3251.
(43) Confalonieri, P.; Volpe, M. C.; Jacob, J.; Maiocchi, S.; Salton, F.; Ruaro, B.; Confalonieri, M.; Braga, L. Regeneration or Repair? The Role of Alveolar Epithelial Cells in the Pathogenesis of Idiopathic Pulmonary Fibrosis (IPF). *Cells* **2022**, *11* (13), 2095.
(44) Mei, Q.; Liu, Z.; Zuo, H.; Yang, Z.; Qu, J. Idiopathic Pulmonary Fibrosis: An Update on Pathogenesis. *Front. Pharmacol.* **2022**, *12*, 797292.
(45) Ogawa, T.; Shichino, S.; Ueha, S.; Matsushima, K. Macrophages in Lung Fibrosis. *Int. Immunol.* **2021**, *33* (12), 665−671.
(46) Selvarajah, B.; Platé, M.; Chambers, R. C. Pulmonary Fibrosis: Emerging Diagnostic and Therapeutic Strategies. *Mol. Aspects Med.* **2023**, *94*, 101227.
(47) Upagupta, C.; Shimbori, C.; Alsilmi, R.; Kolb, M. Matrix Abnormalities in Pulmonary Fibrosis. *Eur. Respir. Rev.* **2018**, *27* (148), 180033.
(48) An, W.; Zhu, J.-W.; Jiang, F.; Jiang, H.; Zhao, J.-L.; Liu, M.-Y.; Li, G.-X.; Shi, X.-G.; Sun, C.; Li, Z.-S. Fibromodulin Is Upregulated by Oxidative Stress through the MAPK/AP-1 Pathway to Promote Pancreatic Stellate Cell Activation. *Pancreatology* **2020**, *20* (2), 278−287.
(49) Mormone, E.; Lu, Y.; Ge, X.; Fiel, M. I.; Nieto, N. Fibromodulin, an Oxidative Stress-Sensitive Proteoglycan, Regulates the Fibrogenic Response to Liver Injury in Mice. *Gastroenterology* **2012**, *142* (3), 612−621.e5.
(50) Batlle, E.; Massagué, J. Transforming Growth Factor-β Signaling in Immunity and Cancer. *Immunity* **2019**, *50* (4), 924−940.
(51) Peng, D.; Fu, M.; Wang, M.; Wei, Y.; Wei, X. Targeting TGF-β Signal Transduction for Fibrosis and Cancer Therapy. *Mol. Cancer* **2022**, *21* (1), 104.
(52) Horan, G. S.; Wood, S.; Ona, V.; Li, D. J.; Lukashev, M. E.; Weinreb, P. H.; Simon, K. J.; Hahm, K.; Allaire, N. E.; Rinaldi, N. J.; Goyal, J.; Feghali-Bostwick, C. A.; Matteson, E. L.; O'Hara, C.; Lafyatis, R.; Davis, G. S.; Huang, X.; Sheppard, D.; Violette, S. M. Partial Inhibition of Integrin Alpha(v)Beta6 Prevents Pulmonary Fibrosis without Exacerbating Inflammation. *Am. J. Respir. Crit. Care Med.* **2008**, *177* (1), 56−65.
(53) Munger, J. S.; Huang, X.; Kawakatsu, H.; Griffiths, M. J.; Dalton, S. L.; Wu, J.; Pittet, J. F.; Kaminski, N.; Garat, C.; Matthay, M. A.; Rifkin, D. B.; Sheppard, D. The Integrin Alpha v Beta 6 Binds and Activates Latent TGF Beta 1: A Mechanism for Regulating Pulmonary Inflammation and Fibrosis. *Cell* **1999**, *96* (3), 319−328.
(54) Andugulapati, S. B.; Gourishetti, K.; Tirunavalli, S. K.; Shaikh, T. B.; Sistla, R. Biochanin-A Ameliorates Pulmonary Fibrosis by Suppressing the TGF-β Mediated EMT, Myofibroblasts Differentiation and Collagen Deposition in in Vitro and in Vivo Systems. *Phytomedicine* **2020**, *78*, 153298.
(55) Chanda, D.; Otoupalova, E.; Smith, S. R.; Volckaert, T.; De Langhe, S. P.; Thannickal, V. J. Developmental Pathways in the Pathogenesis of Lung Fibrosis. *Mol. Aspects Med.* **2019**, *65*, 56−69.
(56) Dadrich, M.; Nicolay, N. H.; Flechsig, P.; Bickelhaupt, S.; Hoeltgen, L.; Roeder, F.; Hauser, K.; Tietz, A.; Jenne, J.; Lopez, R.; Roehrich, M.; Wirkner, U.; Lahn, M.; Huber, P. E. Combined Inhibition of TGFβ and PDGF Signaling Attenuates Radiation-Induced Pulmonary Fibrosis. *Oncoimmunology* **2016**, *5* (5), No. e1123366.

https://doi.org/10.1021/acs.jproteome.4c00715
J. Proteome Res. 2025, 24, 1715−1731

(57) Inui, N.; Sakai, S.; Kitagawa, M. Molecular Pathogenesis of Pulmonary Fibrosis, with Focus on Pathways Related to TGF-β and the Ubiquitin-Proteasome Pathway. *Int. J. Mol. Sci.* **2021**, *22* (11), 6107.
(58) Shi, L.; Dong, N.; Fang, X.; Wang, X. Regulatory mechanisms of TGF-beta 1-induced fibrogenesis of human alveolar epithelial cells (2016). *J. Cell. Mol. Med.* **2017**, *21* (4), 831−833.
(59) Bao, L.; Geng, Z.; Wang, J.; He, L.; Kang, A.; Song, J.; Huang, X.; Zhang, Y.; Liu, Q.; Jiang, T.; Pang, Y.; Niu, Y.; Zhang, R. Attenuated T Cell Activation and Rearrangement of T Cell Receptor β Repertoire in Silica Nanoparticle-Induced Pulmonary Fibrosis of Mice. *Environ. Res.* **2022**, *213*, 113678.
(60) Ding, M.; Zhang, C.; Wang, W.; Wang, P.; Pei, Y.; Wang, N.; Huang, S.; Hao, C.; Yao, W. Silica-Exposed Macrophages-Secreted Exosomal miR125a-5p Induces Th1/Th2 and Treg/Th17 Cell Imbalance and Promotes Fibroblast Transdifferentiation. *Ecotoxicol. Environ. Saf.* **2023**, *267*, 115647.
(61) Lee, S.; Hayashi, H.; Maeda, M.; Chen, Y.; Matsuzaki, H.; Takei-Kumagai, N.; Nishimura, Y.; Fujimoto, W.; Otsuki, T. Environmental Factors Producing Autoimmune Dysregulation–Chronic Activation of T Cells Caused by Silica Exposure. *Immunobiology* **2012**, *217* (7), 743−748.
(62) You, Y.; Wu, X.; Yuan, H.; He, Y.; Chen, Y.; Wang, S.; Min, H.; Chen, J.; Li, C. Crystalline Silica-Induced Recruitment and Immuno-Imbalance of CD4+ Tissue Resident Memory T Cells Promote Silicosis Progression. *Commun. Biol.* **2024**, *7* (1), 971.
(63) Celada, L. J.; Kropski, J. A.; Herazo-Maya, J. D.; Luo, W.; Creecy, A.; Abad, A. T.; Chioma, O. S.; Lee, G.; Hassell, N. E.; Shaginurova, G. I. PD-1 up-Regulation on CD4+ T Cells Promotes Pulmonary Fibrosis through STAT3-Mediated IL-17A and TGF-B1 Production. *Sci. Transl. Med.* **2018**, *10* (460), No. eaar8356.
(64) Ju, Z.; Shao, J.; Zhou, M.; Jin, J.; Pan, H.; Ding, P.; Huang, R. Transcriptomic and Metabolomic Profiling Reveal the P53-Dependent Benzeneacetic Acid Attenuation of Silica-Induced Epithelial-Mesenchymal Transition in Human Bronchial Epithelial Cells. *Cell Biosci.* **2021**, *11* (1), 30.
(65) Gonçalves-de-Albuquerque, C. F.; Silva, A. R.; Burth, P.; Castro-Faria, M. V.; Castro-Faria-Neto, H. C. Acute Respiratory Distress Syndrome: Role of Oleic Acid-Triggered Lung Injury and Inflammation. *Mediators Inflamm.* **2015**, *2015*, 260465.
(66) Beilman, G. Pathogenesis of Oleic Acid-Induced Lung Injury in the Rat: Distribution of Oleic Acid during Injury and Early Endothelial Cell Changes. *Lipids* **1995**, *30* (9), 817−823.
(67) Healy, D. A.; Watson, R. W. G.; Newsholme, P. Polyunsaturated and Monounsaturated Fatty Acids Increase Neutral Lipid Accumulation, Caspase Activation and Apoptosis in a Neutrophil-like, Differentiated HL-60 Cell Line. *Clin. Sci.* **2003**, *104* (2), 171−179.
(68) Martins de Lima, T.; Cury-Boaventura, M. F.; Giannocco, G.; Nunes, M. T.; Curi, R. Comparative Toxicity of Fatty Acids on a Macrophage Cell Line (J774). *Clin. Sci.* **2006**, *111* (5), 307−317.
(69) Martins de Lima, T.; Gorjão, R.; Hatanaka, E.; Cury-Boaventura, M. F.; Portioli Silva, E. P.; Procopio, J.; Curi, R. Mechanisms by Which Fatty Acids Regulate Leucocyte Function. *Clin. Sci.* **2007**, *113* (2), 65−77.
(70) Matute-Bello, G.; Frevert, C. W.; Martin, T. R. Animal Models of Acute Lung Injury. *Am. J. Physiol. Lung Cell Mol. Physiol.* **2008**, *295* (3), L379−399.
(71) Lee, J. D.; Kim, H. Y.; Kang, K.; Jeong, H. G.; Song, M.-K.; Tae, I. H.; Lee, S. H.; Kim, H. R.; Lee, K.; Chae, S.; Hwang, D.; Kim, S.; Kim, H. S.; Kim, K.-B.; Lee, B.-M. Integration of Transcriptomics, Proteomics and Metabolomics Identifies Biomarkers for Pulmonary Injury by Polyhexamethylene Guanidine Phosphate (PHMG-p), a Humidifier Disinfectant, in Rats. *Arch. Toxicol.* **2020**, *94* (3), 887−909.
(72) Gaugg, M. T.; Engler, A.; Bregy, L.; Nussbaumer-Ochsner, Y.; Eiffert, L.; Bruderer, T.; Zenobi, R.; Sinues, P.; Kohler, M. Molecular Breath Analysis Supports Altered Amino Acid Metabolism in Idiopathic Pulmonary Fibrosis. *Respirology* **2019**, *24* (5), 437−444.
(73) Qiu, M.; Qin, L.; Dong, Y.; Ma, J.; Yang, Z.; Gao, Z. The Study of Metabolism and Metabolomics in a Mouse Model of Silica Pulmonary Fibrosis Based on UHPLC-QE-MS. *Artif. Cells, Nanomed., Biotechnol.* **2022**, *50* (1), 322−330.
(74) Cheepala, S.; Hulot, J.-S.; Morgan, J. A.; Sassi, Y.; Zhang, W.; Naren, A. P.; Schuetz, J. D. Cyclic Nucleotide Compartmentalization: Contributions of Phosphodiesterases and ATP-Binding Cassette Transporters. *Annu. Rev. Pharmacol. Toxicol.* **2013**, *53*, 231−253.
(75) Fukuda, Y.; Schuetz, J. D. ABC Transporters and Their Role in Nucleoside and Nucleotide Drug Resistance. *Biochem. Pharmacol.* **2012**, *83* (8), 1073−1083.
(76) Dean, M.; Moitra, K.; Allikmets, R. The Human ATP-Binding Cassette (ABC) Transporter Superfamily. *Hum. Mutat.* **2022**, *43* (9), 1162−1182.
(77) Glavinas, H.; Krajcsi, P.; Cserepes, J.; Sarkadi, B. The Role of ABC Transporters in Drug Resistance, Metabolism and Toxicity. *Curr. Drug Deliv.* **2004**, *1* (1), 27−42.
(78) Alam, A.; Locher, K. P. Structure and Mechanism of Human ABC Transporters. *Annu. Rev. Biophys.* **2023**, *52*, 275−300.
(79) Langmann, T.; Mauerer, R.; Zahn, A.; Moehle, C.; Probst, M.; Stremmel, W.; Schmitz, G. Real-Time Reverse Transcription-PCR Expression Profiling of the Complete Human ATP-Binding Cassette Transporter Superfamily in Various Tissues. *Clin. Chem.* **2003**, *49* (2), 230−238.
(80) Chai, A. B.; Ammit, A. J.; Gelissen, I. C. Examining the Role of ABC Lipid Transporters in Pulmonary Lipid Homeostasis and Inflammation. *Respir. Res.* **2017**, *18* (1), 41.
(81) Bush, A.; Pabary, R. Pulmonary Alveolarproteinosis in Children. *Breathe (Sheff)* **2020**, *16* (2), 200001.
(82) He, P.; Gelissen, I. C.; Ammit, A. J. Regulation of ATP Binding Cassette Transporter A1 (ABCA1) Expression: Cholesterol-Dependent and - Independent Signaling Pathways with Relevance to Inflammatory Lung Disease. *Respir. Res.* **2020**, *21* (1), 250.
(83) Zhang, L.; Huang, P.; Huang, C.; Jiang, L.; Lu, Z.; Wang, P. Varied Clinical Significance of ATP-Binding Cassette C Sub-Family Members for Lung Adenocarcinoma. *Medicine* **2021**, *100* (16), No. e25246.
(84) Draper, D. W.; Gowdy, K. M.; Madenspacher, J. H.; Wilson, R. H.; Whitehead, G. S.; Nakano, H.; Pandiri, A. R.; Foley, J. F.; Remaley, A. T.; Cook, D. N.; Fessler, M. B. ATP Binding Cassette Transporter G1 Deletion Induces IL-17-Dependent Dysregulation of Pulmonary Adaptive Immunity. *J. Immunol.* **2012**, *188* (11), 5327−5336.
(85) Draper, D. W.; Madenspacher, J. H.; Dixon, D.; King, D. H.; Remaley, A. T.; Fessler, M. B. ATP-Binding Cassette Transporter G1 Deficiency Dysregulates Host Defense in the Lung. *Am. J. Respir. Crit. Care Med.* **2010**, *182* (3), 404−412.
(86) Aguiar, J. A.; Tamminga, A.; Lobb, B.; Huff, R. D.; Nguyen, J. P.; Kim, Y.; Dvorkin-Gheva, A.; Stampfli, M. R.; Doxey, A. C.; Hirota, J. A. The Impact of Cigarette Smoke Exposure, COPD, or Asthma Status on ABC Transporter Gene Expression in Human Airway Epithelial Cells. *Sci. Rep.* **2019**, *9* (1), 153.

https://doi.org/10.1021/acs.jproteome.4c00715
J. Proteome Res. 2025, 24, 1715−1731